Received: 6 August 2021 | Revised: 19 May 2022 | Accepted: 20 May 2022

DOI: 10.1002/eqe.3692

RESEARCH ARTICLE

WILEY

# Non-linear dynamic model of a two-bodies vertical spanning wall elastically restrained at the top

**Sanjeev Prajapati**[1] | **Giacomo Destro Bisol**[2] | **Omar AlShawa**[2] | **Luigi Sorrentino**[2]

[1]City of Kalgoorlie Boulder Council, Kalgoorlie WA, Australia

[2]Department of Structural and Geotechnical Engineering, Sapienza University of Rome, Rome, Italy

**Correspondence**
Omar AlShawa, Department of Structural and Geotechnical Engineering, Sapienza University of Rome, via Antonio Gramsci 53, 00197 Rome, Italy
Email: omar.alshawa@uniroma1.it

**Abstract**

Understanding the out-of-plane behavior of unreinforced masonry walls is crucial in seismic assessment of existing buildings. Here, the dynamic response of a vertical spanning strip wall, connected to a flexible diaphragm at the top, is investigated. Despite the simplicity of the model, two rocking rigid bodies elastically restrained at the top, the dynamic response is highly nonlinear. This behavior is due to different phenomena: when in motion the system may assume different configurations, with the transition between them due either to impacts or crack opening caused by ground acceleration. An analytical model capable to capture the complex dynamic response of the system is implemented. The equations of motion are first derived, using variational methods, then the events that the system can undergo during motion are studied. Finally, in order to show the potential of the model, some numerical exemplifications are presented applying an earthquake record and a sine pulse to the system.

**KEYWORDS**

event strategy, flexible diaphragm, impulsive energy dissipation, pattern change, unreinforced masonry, vibration pattern

## 1 | INTRODUCTION

In unreinforced masonry (URM) buildings without box behavior, the out-of-plane (OOP) mechanisms are among the most dangerous events that can occur during earthquakes.[1] The quality of the masonry plays an essential role in the type and in the magnitude of damage following an earthquake. The masonry must have adequate quality to resist horizontal actions and to transfer vertical loads at the same time and the structure, or parts of it, must have a monolithic behavior, otherwise masonry disintegration may occur.[2] The OOP behavior of a wall significantly changes if it is connected to horizontal structural elements (Figure 1A). The collapse, in this case, could take place for slipping/failure of the diaphragm or for overturning of the wall, following the formation of a crack at an intermediate height between the base and the top as observed after earthquakes in several countries.[3–5] The height, at which the wall breaks, depends on the ratio between the weight due to the diaphragm and that of the wall. The larger the weight acting at the top, compared to that of the wall, the more the crack moves downwards.[6]

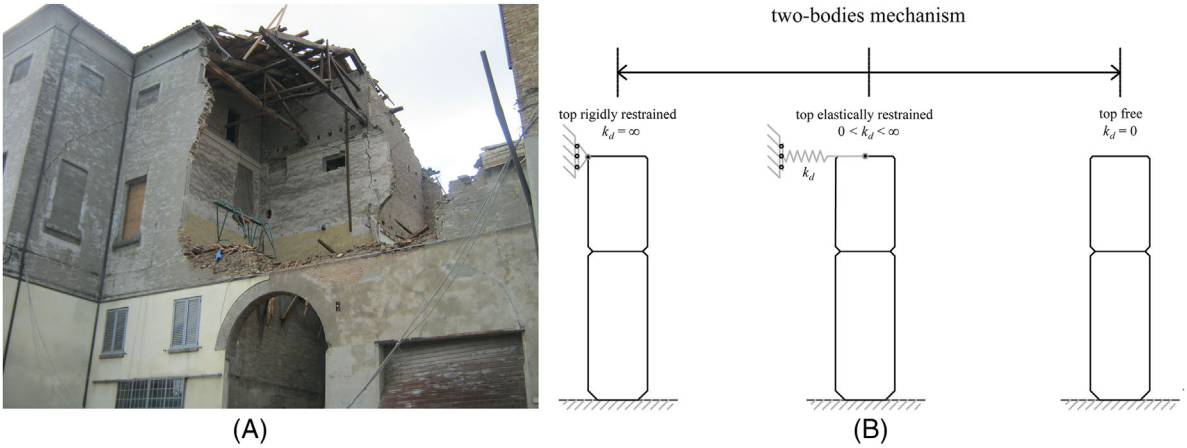


**FIGURE 1** Out-of-plane failure of a slender facade: (A) Emilia (Italy) 2012; (B) top boundary conditions

If the floor is sufficiently stiff, the top restraint can be assumed as rigid, thus simplifying the problem statement and solution. Baggio and Masiani[7] and Doherty et al.[8] carried out experimental tests on this configuration. Based on these tests, Doherty et al.,[8] as well as Lam et al.[9] and Griffith et al.[10] developed an analytical model with one degree of freedom (DOF), accounting in a simplified way for the geometrical non linearity of the wall. These studies highlighted the higher accuracy of the displacement-based safety assessment approach compared with the force-based one. Sorrentino et al.[11] studied a vertical spanning strip wall as a coupled rocking rigid body assembly. The analytical model accounts explicitly for the effect of the thickness and, consequently, for the geometrical non-linearities. Further experimental campaigns were performed by Wilhelm et al.[12] and Meisl et al.[13] The former study concluded that the main crack formed at two-thirds of the height of the wall and the boundary conditions strongly influence its OOP performance. The latter confirmed the trend of a wall to crack and to behave like an assembly of rocking rigid bodies. Derakhshan et al.[14] performed a set of quasi-static tests on eight full-scale URM walls. The load was applied by means of a system of airbags to ensure a uniform lateral pressure. The tests found an average crack height ratio of 0.58. The analytical model with the top rigidly restrained was recently studied by DeJong and Dimitrakopoulos,[15] as well as by Godio and Beyer.[16] The former explored the effect of linearizing equations of motion, while the latter, using a discrete element method, highlighted again the higher accuracy of the equivalent-static displacement-based assessment method compared with the force-based one.

DeJong and Dimitrakopoulos[15] represent an example of more general numerical approaches to study the OOP behavior of a masonry wall, which can be found in the literature and that are mainly concerned with a configuration where the top is rigidly restrained. Other examples of the application of the discrete element method to OOP response are in refs. [17–19] A new formulation of the finite element method was used in Noor-E-Khuda et al.[20] to evaluate the OOP vertical spanning mechanisms of masonry walls. In the applied element method, a masonry element is discretized in rigid units connected by springs,[21] consequently it is possible to capture the OOP behavior, particularly in the pre-cracked phase. The flexural OOP mechanism was studied also using a macro-distinct element model,[22] where the wall was subdivided in an assembly of macro-blocks connected by springs. The procedure was capable to capture several failure mechanisms, including the crushing of masonry. A macro-element formulation, previously developed to model the in-plane response of walls, was updated to evaluate the response of OOP mechanisms and identify the collapse mechanism.[23]

When the horizontal diaphragm is not sufficiently stiff, a flexible restraint at the top must be assumed.[24] In this case, the system has two DOFs, as happens in a system of two stacked bodies free at the top (Figure 1B), studied by Psycharis[25] and by Spanos et al.[26] In such a case the complexity of the problem increases considerably because four modes (or patterns) are possible and the transition from one pattern to another is determined by the balance between overturning and resisting moments or by impacts.[27] Kounadis et al.[28] studied the same problem of Spanos et al.,[26] linearizing the equation of motion in order to derive the closed-form solution for the system under pulse excitations. It was found that overturning occurs after an impact for comparatively large values of excitation frequency, otherwise overturning takes place without any impact. Papaloizou and Komodromos[29] developed a discrete element method based software by using modern object-oriented design programming, validating their code with Spanos et al.[26] Furthermore, similarly to what proposed by Ishiyama[30] for a single-body system, Chatzis et al.[31] updated the model in Spanos et al.,[26] in order to consider impact forces distributed over an area rather than concentrated along an edge, showing that the latter assumption is not conservative.

OOP flexure of a wall with elastic restraints was studied by the ABK consortium[32] that performed dynamic tests on 22 natural-scale URM walls. Flexibility of diaphragms was accounted for by using two independent displacement-controlled actuators, undergoing estimated input motions at the top and the bottom of the wall. The tests showed that the OOP capacity was correlated to peak velocities and that a wall can rock after cracking without necessarily overturning. Simsir et al.[33] performed shake table tests on a half-scale single-story URM building with a diaphragm of varying stiffness, highlighting its strong influence in the response. Further, neglecting the geometric non-linearity, a simplified model was developed. The model considered at the top a lumped mass and an elastic spring to represent the diaphragm, along with rotational springs at the crack and at the base. Derakhshan et al.[34] studied single-story and two-story one-way spanning walls connected to flexible diaphragms. The derived model considered the thickness of the wall negligible. Similar assumptions are shared by Gabellieri et al.[35] for a single-story URM wall. Penner and Elwood[36] performed full-scale shaking table tests on five masonry wall specimens. The specimens were connected to a steel frame by elastic springs. The inertia forces on the wall and the reactions of the springs initiate the rocking motion as two semi-rigid bodies, developing a crack at intermediate height. Landi et al.[37] developed a model taking into account the thickness of the wall and simplifying the problem using the hypothesis of small displacements. Derakhshan et al.[38] developed a three DOFs model, in order to take into account the thickness of the wall and the deformation of a base diaphragm. Both numerical models highlighted the strong influence of diaphragm stiffness on the response of the wall.

In the literature are present models accounting for geometric non-linearities in the case of a wall rigidly restrained at the top. The same can be stated for the model free at the top, which considers four different patterns. No model accounting for all previously mentioned phenomena, is available. Therefore, it is proposed a model formed by two bodies of finite thickness and elastically restrained at the top. In the following sections, equations of motion are derived for all vibration patterns, their possible transitions are mapped, and an event strategy is used to build the numerical model.

## 2 | DESCRIPTION OF THE SYSTEM

The OOP response of a vertical spanning wall, connected to a flexible diaphragm, is modeled by means of two rigid bodies restrained at the top by an elastic spring (Figure 2). Friction is assumed large enough to prevent any sliding. The heights of

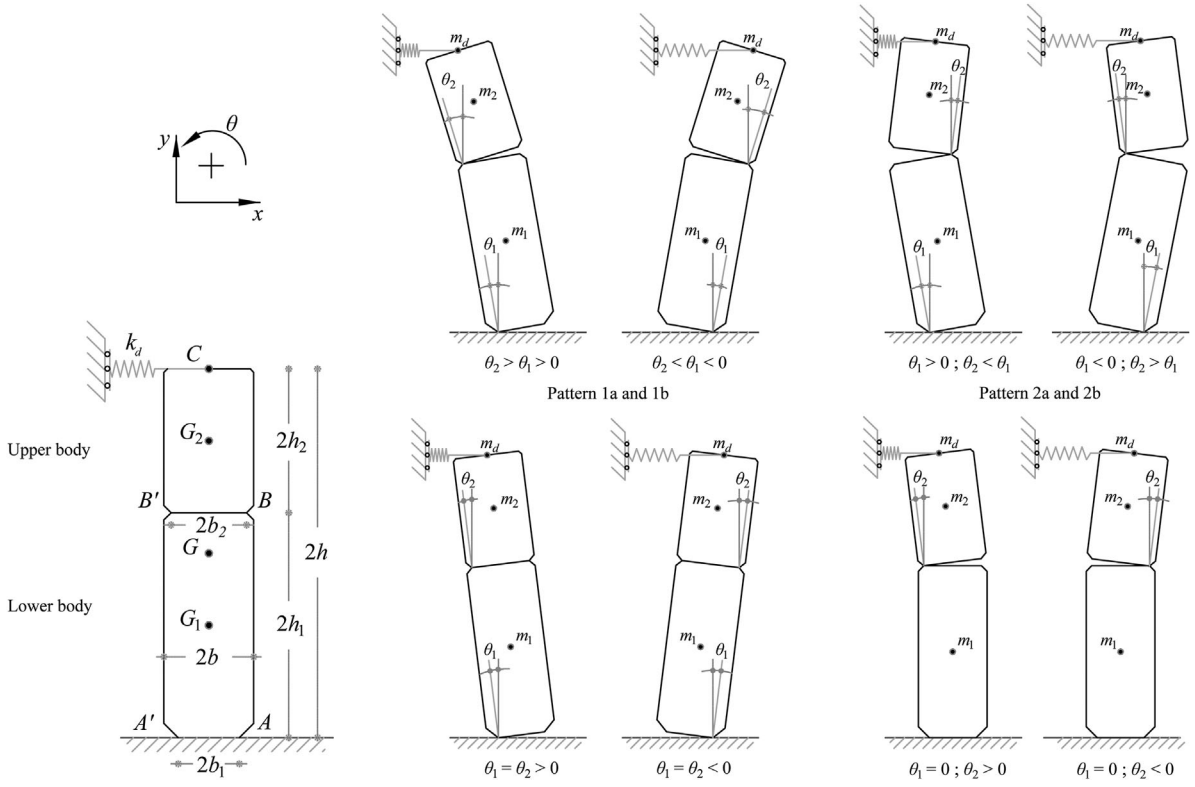


**FIGURE 2** Elastically restrained two-bodies system and possible motion patterns

the lower and upper bodies are $2h_1$ and $2h_2$, respectively, while $2h$ is the total height of the wall. The thickness of the wall is $2b$ but the thicknesses of the interfaces at the bottom of the lower and upper bodies are in general different and equal to $2b_1$ and $2b_2$, respectively. This difference is related to the internal forces acting at pivots, which are different because related to the weight of the wall section above each crack. These forces cause a different extent of masonry crushing and, consequently, interfaces of different thickness. The masses of the lower and upper bodies are $m_1$ and $m_2$, respectively, while $m$ is the total mass of the wall, the lumped mass of the diaphragm is $m_d$ and its stiffness is $k_d$. The vertical spanning strip wall, attached to a flexible top restraint, undergoes four different patterns, each having symmetric cases (Figure 2).

The formulation of the equation of motion of complex systems can rely on energy principles.[39] For each pattern, the analytical equation of motion is formulated within a Lagrangian approach to avoid the computation of internal forces.[40] This approach allows for the use of generalized coordinates to describe the motion of the system and to define all kinematic quantities. In the case of rocking rigid bodies, it is convenient to describe the movement of the system (therefore of each point) by means of rotations, namely $\theta_1$ for the lower body and $\theta_2$ for the upper body. The scalar parameters of kinetic energy $T$ and potential energy $V$, as well as non-conservative generalized forces $Q$ are computed, in order to assemble the Lagrangian equation of motion:

$$\frac{d}{dt}\left(\frac{\partial L}{\partial \dot{\theta}_i}\right) - \frac{\partial L}{\partial \theta_i} = Q_i \quad i = 1,\ 2 \tag{1}$$

where $t$ is the time, $L = T - V$, $\dot{\theta}_i$ is the angular velocity, $\theta_i$ is the rotation, and $i = 1$ or 2 makes reference to the lower or the upper body, respectively.

In the case at hand, the kinetic energy is equal to:

$$T = \sum_{i=1}^{2}\left[\frac{1}{2}\left(m_i\left|\mathbf{v}_{G_i}\right|^2 + I_{G_i}\dot{\theta}_i\right)\right] + \frac{1}{2}m_d|\mathbf{v}_C|^2 \text{where } |\mathbf{v}| = \sqrt{{v_x}^2 + {v_y}^2} \tag{2}$$

and $m_i$ is the mass of the $i$th body, $I_{Gi}$ is the polar inertia moment of the $i$th body about its center of mass $G_i$, $\mathbf{v}_{Gi}$ and $\mathbf{v}_C$ are respectively the velocity vectors of the $i$th center of mass and of point $C$ where the diaphragm mass is applied. Scalar components of vectors make reference to $x$, $y$ axes in Figure 2.

The potential energy is equal to:

$$V = \sum_{i=1}^{2} g m_i p_{G_i,y} + g m_d p_{C,y} + \frac{1}{2}k_d s_{C,x}^2 \tag{3}$$

where $g$ is the gravity acceleration, $p_{Gi,y}$ and $p_{C,y}$ are the vertical components of the position vectors of the center of mass of the $i$th body and of point $C$, respectively, while $s_{C,x}$ is the horizontal component of the displacement vector $\mathbf{s}_C$ of point $C$.

Examples of non-conservative forces are air resistance, friction, and some types of impressed forces. In the present case, this type of forces are generated by the horizontal $\ddot{x}_g$ and vertical $\ddot{y}_g$ components of the seismic ground acceleration. The non-conservative generalized forces $Q_i$ are obtained by deriving the virtual work $W$:

$$Q_i = \sum\nolimits_{i=1}^{2}\frac{\partial W}{\partial \theta_i} \text{ where } W = -\ddot{x}_g\left(\sum\nolimits_{i=1}^{2} m_i s_{G_i,x} + m_d s_{C,x}\right) - \ddot{y}_g\left(\sum\nolimits_{i=1}^{2} m_i s_{G_i,y} + m_d s_{C,y}\right) \tag{4}$$

and $\mathbf{s}_{Gi}$ is the displacement vector of the $i$th center of mass.

Once all the scalar parameters (energies and generalized forces) are evaluated, it is necessary to insert them in the two Lagrangian equations of motion (one for each generalized coordinate). Noting that the potential energy $V$ does not depend on velocity, it is possible to rewrite the Lagrangian equation of motion (1) in the following form:

$$\begin{cases} \dfrac{d}{dt}\left(\dfrac{\partial T}{\partial \dot{\theta}_1}\right) - \dfrac{\partial T}{\partial \theta_1} + \dfrac{\partial V}{\partial \theta_1} = Q_1 \\ \dfrac{d}{dt}\left(\dfrac{\partial T}{\partial \dot{\theta}_2}\right) - \dfrac{\partial T}{\partial \theta_2} + \dfrac{\partial V}{\partial \theta_2} = Q_2 \end{cases} \tag{5}$$

Once the Lagrangian equations of motion are assembled, it is necessary to perform the partial and total derivation operations, in order to obtain a system of two non-linear differential equations of the second order in the two Lagrangian unknowns $\theta_1$ and $\theta_2$. Subsequently the two equations are manipulated and rewritten in matrix form:

$$\mathbf{M}\,\ddot{\theta} = \mathbf{F};\ \begin{bmatrix} M_{11} & M_{12} \\ M_{21} & M_{22} \end{bmatrix} \cdot \begin{Bmatrix} \ddot{\theta}_1 \\ \ddot{\theta}_2 \end{Bmatrix} = \begin{Bmatrix} F_1 \\ F_2 \end{Bmatrix} \tag{6}$$

where $\mathbf{M}$ is the mass matrix, $\ddot{\theta}$ is the angular acceleration vector, and $\mathbf{F}$ is the vector that contains the low-order derivatives (rotations and angular velocities) as well as the known terms. Quantities $M_{jk}$, $F_i$ are defined in the following section and in Appendix A for each pattern.

## 3 | EQUATIONS OF MOTION

As noted above, the system can oscillate in different patterns (Figure 2), all characterized by their own equations of motion calculated by means of the aforementioned procedure. The response of the system is extremely non-linear, not only for the intrinsic geometric non-linearity of the equations of motion but also for the change of rocking hinge and due to the presence of different patterns, which may involve a change in the number of DOFs during motion.

Pattern 1 takes place when $|\theta_2| > |\theta_1| > 0$, that is when the rotations $\theta_1$ and $\theta_2$ have the same sign but the modulus of $\theta_2$ is greater than that of $\theta_1$. In this case the system has two DOFs, therefore the equation of motion consists in a system of two differential equations in the two Lagrangian parameters. Using the matrix notation of Equation (6), it is possible to divide the equation of motion in two parts: the mass matrix, whose components are:

$$\begin{aligned} M_{11} &= I_{G_1} + b_1^2 A_1 - (2b_1 - b_2)\, b_2 A_2 + h_1^2 A_5; \quad M_{22} = I_{G_2} + b_2^2 A_2 + h_2^2 A_6 \\ M_{12} &= M_{21} = \mathrm{S}_\theta\ [(b_1 - b_2)\, h_2 A_4 - 2b_2 h_1 A_2] \sin(\theta_1 - \theta_2) + [(b_1 - b_2)\, b_2 A_2 - 2h_1 h_2 A_4] \cos(\theta_1 - \theta_2) \end{aligned} \tag{7}$$

and the vector $\mathbf{F}$ whose components are:

$$\begin{aligned} F_1 &= \{\sin(\theta_1 - \theta_2)\,[-(b_1 - b_2)\, b_2 A_2 - 2h_1 h_2 A_4] + \mathrm{S}_\theta \cos(\theta_1 - \theta_2)\,[(b_1 - b_2)\, h_2 A_4 - 2b_2 h_1 A_2]\}\,\dot{\theta}_2 - \\ &[(b_1 - b_2)\sin\theta_1 + \mathrm{S}_\theta 2h_1 \cos\theta_1]\,[b_1(1 - \cos\theta_1) + b_2(\cos\theta_1 - \cos\theta_2) + \mathrm{S}_\theta 2h_1 \sin\theta_1 + \mathrm{S}_\theta 2h_2 \sin\theta_2]\,k_d \\ &+ [\mathrm{S}_\theta (b_1 A_1 - b_2 A_2)\sin\theta_1 + h_1 A_3 \cos\theta_1]\,\ddot{x}_g + [h_1 A_3 \sin\theta_1 - \mathrm{S}_\theta (b_1 A_1 - b_2 A_2)\cos\theta_1]\,(g + \ddot{y}_g) \\ F_2 &= \{\sin(\theta_1 - \theta_2)\,[(b_1 - b_2)\, b_2 A_2 + 2h_1 h_2 A_4] + \mathrm{S}_\theta \cos(\theta_1 - \theta_2)\,[2b_2 h_1 A_2 - (b_1 - b_2)\, h_2 A_4]\}\,\dot{\theta}_1 - \\ &(2h_2 \cos\theta_2 + \mathrm{S}_\theta b_2 \sin\theta_2)\,[\mathrm{S}_\theta b_1 (1 - \cos\theta_1) + \mathrm{S}_\theta b_2 (\cos\theta_1 - \cos\theta_2) + 2h_1 \sin\theta_1 + 2h_2 \sin\theta_2]\,k_d + \\ &(\mathrm{S}_\theta b_2 A_2 \sin\theta_2 + h_2 A_4 \cos\theta_2)\,\ddot{x}_g + (h_2 A_4 \sin\theta_2 - \mathrm{S}_\theta b_2 A_2 \cos\theta_2)\,(g + \ddot{y}_g) \end{aligned} \tag{8}$$

where $A_i$ terms have units of mass and are equal to:

$$\begin{aligned} &A_1 = m_1 + m_2 + m_d\ ; \quad A_2 = m_2 + m_d\ ; \quad A_3 = m_1 + 2m_2 + 2m_d; \quad A_4 = m_2 + 2m_d; \\ &A_5 = m_1 + 4m_2 + 4m_d; \quad A_6 = m_2 + 4m_d; \qquad A_7 = m + 2m_d; \qquad A_8 = m + 4m_d \end{aligned} \tag{9}$$

and $\mathrm{S}_\theta$ is the sign function:

$$\mathrm{S}_\theta = 1 \text{ if } \theta > 0 \text{ or } \mathrm{S}_\theta = -1 \text{ if } \theta < 0\ ; (\theta \equiv \theta_1 \text{ in pattern 1 and 2};\ \theta \equiv \theta_2 \text{ in pattern 4})\,. \tag{10}$$

When the rotation of the lower body becomes $\theta_1 = 0$ or $\theta_1 = \theta_2$ an impact occurs, making the equations of motion not valid anymore. Special attention to this case will be paid in a following section, where a specific formulation will be derived. In Equations (7) and (8) the half-thicknesses of the two interfaces are kept different ($b_1 \neq b_2$) to account for a different extent of masonry crushing at the two cracks. If such difference is negligible the two equations can be markedly

simplified:

$$M_{11} = I_{G_1} + \mathrm{b}^2 m_1 + h_1^2 A_5; \quad M_{22} = I_{G_2} + \mathrm{b}^2 A_2 + h_2^2 A_6$$
$$M_{12} = M_{21} = -2h_1 \left[\mathrm{S}_\theta b A_2 \sin(\theta_1 - \theta_2) + h_2 A_4 \cos(\theta_1 - \theta_2)\right] \tag{11}$$

$$\begin{aligned} F_1 &= -2h_1 \left[h_2 A_4 \sin(\theta_1 - \theta_2) + \mathrm{S}_\theta b A_2 \cos(\theta_1 - \theta_2)\right] \dot{\theta}_2 - \mathrm{S}_\theta 2h_1 \cos\theta_1 \\ &[b(1 - \cos\theta_2) + \mathrm{S}_\theta 2h_1 \sin\theta_1 + \mathrm{S}_\theta 2h_2 \sin\theta_2]\, k_d + [\mathrm{S}_\theta b m_1 \sin\theta_1 + A_3 \cos\theta_1]\, \ddot{x}_g + \\ &[h_1 A_3 \sin\theta_1 - \mathrm{S}_\theta b m_1 \cos\theta_1]\,(g + \ddot{y}_g) \\ F_2 &= 2h_1 \left[h_2 A_4 \sin(\theta_1 - \theta_2) + \mathrm{S}_\theta b A_2 \cos(\theta_1 - \theta_2)\right] \dot{\theta}_1 - (2h_2 \cos\theta_2 + \mathrm{S}_\theta b \sin\theta_2) \\ &[\mathrm{S}_\theta b(1 - \cos\theta_2) + 2h_1 \sin\theta_1 + 2h_2 \sin\theta_2]\, k_d + (\mathrm{S}_\theta b A_2 \sin\theta_2 + h_2 A_4 \cos\theta_2)\, \ddot{x}_g + \\ &(h_2 A_4 \sin\theta_2 - \mathrm{S}_\theta b A_2 \cos\theta_2)\,(g + \ddot{y}_g) \end{aligned} \tag{12}$$

For the components of the matrix equations of motion of patterns 2, 3, and 4 (Figure 2) refer to Appendix A.

## 4 | PATTERN CHANGE DUE TO ACCELERATIONS

A pattern change can occur for two reasons: (a) sudden accelerations,[41] (b) impacts, with the latter case involving the lower body hitting the foundation ($\theta_1 = 0$), or the upper body ($\theta_1 = \theta_2$). These pattern changes were already studied by Spanos et al.,[26] except for those from pattern 1 to pattern 4 and from pattern 2 to pattern 4 considered hereinafter. Moreover, in the following the contribution of the top diaphragm is appropriately introduced.

In order to detect pattern changes occurring without impact, the estimation of a threshold acceleration is required. To this end, it is necessary to compare the external moment $M_E$, which generally tends to overturn the bodies, with the internal moment $M_I$, which generally stabilizes the bodies. External moments are due to the seismic inertia forces and to the restraint elastic force. The effect of these forces is computed in the external acceleration vector $\mathbf{a}_E$ and in the external forces vector $\mathbf{f}_E$:

$$\mathbf{a}_E = \left\{-\ddot{x}_g,\ -\ddot{y}_g - g,\ 0\right\}\ ; \quad \mathbf{f}_E = \left\{-k_d s_{CR,x},\ 0,\ 0\right\} \tag{13}$$

where $s_{CR,x}$ is the horizontal component of point $C$ displacement vector with respect to the generic rotation center $R$.

It is important to notice that the acceleration and force vectors are computed in the current pattern (hence, with respect to the generic rotation center $R$), while the moments are computed with respect to the prospective pattern in which the system could change if the acceleration is strong enough (generic rotation center $O$). Hence, the external moment is calculated as follows:

$$M_E = \sum_{i=1}^{2} m_i \left(\mathbf{p}_{G_i O} \times \mathbf{a}_\mathrm{E}\right) + m_d \left(\mathbf{p}_{CO} \times a_E\right) + \mathbf{p}_{CO} \times \mathbf{f}_E \tag{14}$$

where $\times$ is the vector product operator.

Concerning the internal moment, the accelerations of the masses, with respect to the generic center of rotation $R$ (before the pattern change) must be determined. Because of the rotational motion, the acceleration of the center of mass $G_2$ rotating about $R$ has a normal component directed from $G_2$ toward $R$ and a tangential component perpendicular to $G_2R$.[42] The two components of this acceleration can be written in vectorial form, with respect to the general reference system, as:

$$\mathbf{a}_{G_2R,n} = -\mathbf{p}_{G_2R}\dot{\theta}_i^2; \quad \mathbf{a}_{G_2R,t} = \mathbf{p}_{G_2R} \times \left(-\left\{0,\ 0,\ \ddot{\theta}_i\right\}\right) \tag{15}$$

where $\mathbf{a}_{G_2R,n}$ and $\mathbf{a}_{G_2R,t}$ are respectively the normal and the tangential acceleration vectors of point $G_2$ that rotates about $R$ (Figure 3).

**FIGURE 3** Internal moment calculation

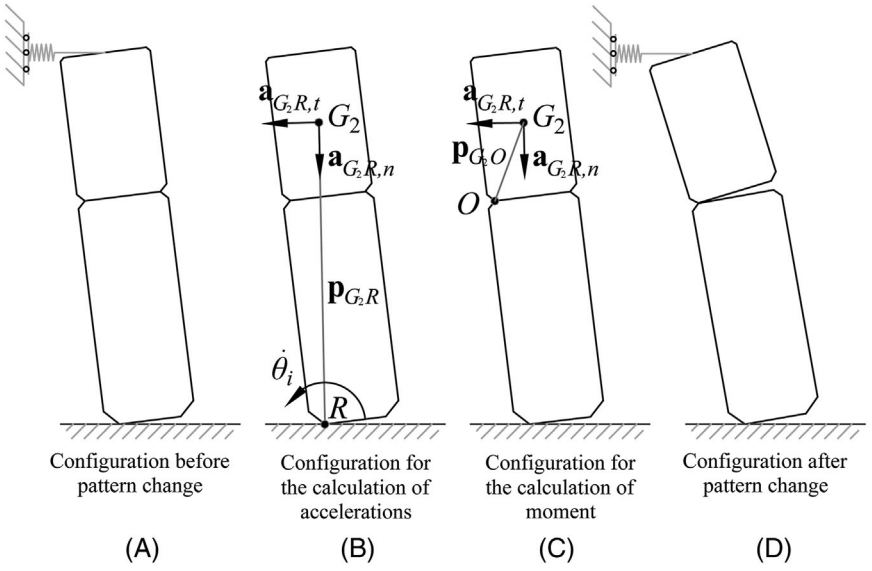


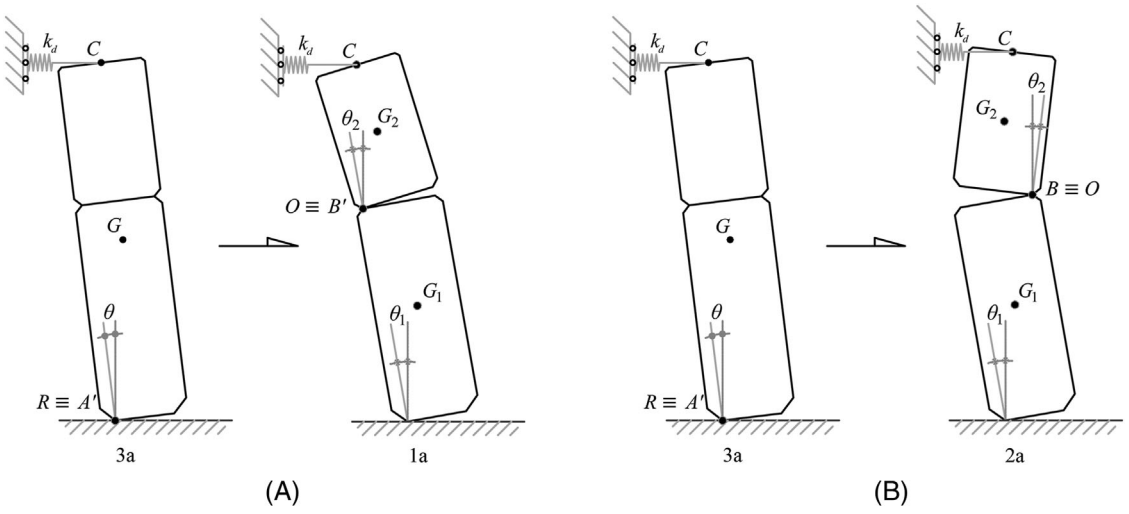


**FIGURE 4** Transition: (A) from pattern 3a to pattern 1a; (B) from pattern 3a to pattern 2a

Once the accelerations of the centers of mass are computed, the internal moment $M_I$ about the rotation center $O$ can be determined as:

$$M_I = I_{G_2}\,\ddot{\theta}_2 + m_i\left(\mathbf{p}_{G_2O}\times\mathbf{a}_{G_2R,n} + \mathbf{p}_{G_2O}\times\mathbf{a}_{G_2R,\mathrm{t}}\right) + m_d\left(\mathbf{p}_{CO}\times\mathbf{a}_{CR,n} + \mathbf{p}_{CO}\times\mathbf{a}_{CR,t}\right) \tag{16}$$

To determine the threshold acceleration causing pattern change, it is sufficient to equal the external and internal moments and to solve with respect to the horizontal acceleration. Pattern changes, due to sudden accelerations, are described below, where only the positive cases are analyzed. However, the threshold accelerations are valid also for the negative cases using the appropriate value for the sign function.

When the system is moving in pattern 3a, if the acceleration is strong enough the crack between upper and lower bodies opens and the system moves according to pattern 1a (the external and internal moments are computed with respect to this configuration). The threshold acceleration to change from one pattern to the other (Figure 4A) is:

$$\begin{aligned}\ddot{x}_{3,1} = {} & \frac{1}{\mathrm{S}_\theta b_2 A_2 \sin\theta + h_2 A_4 \cos\theta} \\ & \Big\{\left[I_{G_2} + b_1 b_2 A_2 + 2h_1 h_2 A_4 + h_2^2 A_6\right]\ddot{\theta}_2 - \mathrm{S}_\theta\left[2h_1 b_2 A_2 + (b_2 - b_1)\,h_2 A_4\right]\dot{\theta}_2^2 + \\ & \left[(2h_2\cos\theta + \mathrm{S}_\theta b_2 \sin\theta)\left(\mathrm{S}_\theta b_1 - \mathrm{S}_\theta b_1\cos\theta + 2h\sin\theta\right)\right]k_d - \left[h_2 A_4 \sin\theta - \mathrm{S}_\theta b_2 A_2\cos\theta\right]\left(g + \ddot{y}_g\right)\Big\}\end{aligned} \tag{17}$$

**TABLE 1** Pattern changes due to acceleration exceeding threshold

| From | Event | To | From | Event | To |
|---|---|---|---|---|---|
| 3a | $\ddot{x}_{3,1} \leq \ddot{x}_g(t)$ | 1a | 3b | $\ddot{x}_{3,1} \geq \ddot{x}_g(t)$ | 1b |
| 3a | $\ddot{x}_{3,2} \geq \ddot{x}_g(t)$ | 2a | 3b | $\ddot{x}_{3,2} \leq \ddot{x}_g(t)$ | 2b |
| 4a | $\ddot{x}_{4,1} \leq \ddot{x}_g(t)$ | 1a | 4b | $\ddot{x}_{4,1} \geq \ddot{x}_g(t)$ | 1b |
| 4a | $\ddot{x}_{4,2} \geq \ddot{x}_g(t)$ | 2b | 4b | $\ddot{x}_{4,2} \leq \ddot{x}_g(t)$ | 2a |

When the system is moving in pattern 3a, due to a sudden excitation the middle crack can open, and the upper body can move in the opposite direction compared to the lower one, so that the system moves according to pattern 2a. The change from one pattern to the other (Figure 4B) requires an acceleration greater than or equal to:

$$\begin{aligned}\ddot{x}_{3,2} = & \frac{1}{h_2 A_4 \cos\theta - \mathrm{S}_\theta b_2 A_2 \sin\theta} \\ & \Big\{ \left[ I_{G_2} - b_1 b_2 A_2 + 2h_1 h_2 A_4 + h_2^2 A_6 \right] \ddot{\theta} + \mathrm{S}_\theta \left[ 2h_1 b_2 A_2 + (b_2 + b_1) h_2 A_4 \right] \dot{\theta}^2 + \\ & \left[ (2h_2 \cos\theta - \mathrm{S}_\theta b_2 \sin\theta) (\mathrm{S}_\theta b_1 - \mathrm{S}_\theta b_1 \cos\theta + 2h \sin\theta) \right] k_d \; - \left[ \mathrm{S}_\theta b_2 A_2 \cos\theta + h_2 A_4 \sin\theta \right] \left( g + \ddot{y}_g \right) \Big\}\end{aligned} \tag{18}$$

Accelerations involving a pattern change without impact when the system is moving according to pattern 4a or 4b are given in Appendix B. In Table 1 the pattern changes related to accelerations exceeding a threshold are summarized accounting for positive and negative values.

## 5 | PATTERN CHANGE DUE TO IMPACTS

As previously mentioned, during motion impact phenomena may occur. In the considered system, formed by two blocks, impacts take place between the lower body and the foundation (when $\theta_1 = 0$) or between the two bodies (when $\theta_1 = \theta_2$ ). In such cases an impact occurs, with consequent energy loss.[27] Impacts are extremely complex events and involve interrelation between many parameters. In this case, in order to simplify the problem, the following assumptions are stipulated: (a) the impact process is characterized using particle mechanics, so that the entire mass of the body is lumped at the center of mass. This approach allows to describe the motion at impact of every point of the body using the kinematic and kinetic relations associated with the center of mass,[43] and to use the equations of impulse and momentum; (b) impacts are based on deformations of the bodies being negligibly small and, consequently, the forces can be considered as impulsive and the impact period as instantaneous. During this instantaneous impact there are changes in the velocities of the bodies, but no change in configuration[44]; (c) the bodies can rock only about the corners so that the impacts are punctual; (d) during the impact, the non-impulsive forces (such as body weight) are negligible, because much smaller than impulsive forces due to the impact; (e) only one impact can occur at a given instant, consequently for instance, transition from pattern 1a to 1b is not possible because it would involve two impacts at the same time.

The impacts lead to pattern and angular velocities changes. To determine velocities after impact the angular moments of the system in the instant before and after the impact must be computed. In accordance with assumption (a) the classical theory of rigid body dynamics is used, so that the angular momentum $H_p$ of a body about the generic point $P$ is:

$$H_P = H_G + m \left( \mathbf{p}_{G,P} \times \mathbf{v}_G \right) \text{ where } H_G = I_G \, \dot{\theta} \tag{19}$$

and $I_G$ is the polar moment of inertia of the body about its center of mass $G$, $\dot{\theta}$ the angular velocity of the body, $\mathbf{v}_G$ the linear velocity of the center of mass, and $\mathbf{p}_{G,N}$ is the position vector from the generic rotation center $N$ to the center of mass.

Then, given the assumptions (b), (c), and (d) the principle of conservation of the angular momentum is used to compute the angular velocities after the impact. The angular momentum of the system $H_{\text{sys}}$ can be computed as:

$$H_{\text{sys}}^- = H_{\text{sys}}^+ \text{ where } H_{\text{sys}} = H_1 + H_2 \tag{20}$$

where the superscripts (–) and (+) indicate respectively the conditions before and after impact, $H_1$ is the angular momentum of the lower body and $H_2$ is the angular momentum of the upper body alone.

If, after the impact, the system moves in pattern 1 or 2 the new velocities of the two bodies must be determined. In this case, Equation (20) holds two unknowns and a second equation must be introduced. Considering the conservation of the angular momentum of the upper body alone, with respect to the point around which it is rotating, a second relation is determined as:

$$H_{\text{top}}^{-} = H_{\text{top}}^{+} \tag{21}$$

This approach is justified because the two bodies are connected only by one of the two corners ($B$ or $B'$), thus all the impact forces are transmitted through this point. Therefore, if the angular momentum is calculated about it, the contribution of the impact force is zero.[26] In the case of a system of two rigid bodies with the flexible diaphragm at the top, the angular momentum $H_{A,\text{sys}}$ with respect to the point $A$ (or $A'$ in the case of negative rotation of the lower body) is:

$$H_{A,\text{sys}} = \sum_{i=1}^{2} I_{G_i}\dot{\theta}_i + \sum_{i=1}^{2} m_i \left(\mathbf{p}_{G_i,A} \times \mathbf{v}_{G_i}\right) + m_d \left(\mathbf{p}_{C,A} \times \mathbf{v}_C\right) \tag{22}$$

Similarly, considering only the upper body, it is possible to write the angular momentum with respect to the generic contact point $B$ (or $B'$ when relevant) as:

$$H_{B,\text{top}} = I_{G_2}\dot{\theta}_2 + m_2 \left(\mathbf{p}_{G_2,A} \times \mathbf{v}_{G_2}\right) + m_d \left(\mathbf{p}_{C,A} \times \mathbf{v}_C\right) \tag{23}$$

Once angular momentums before and after the impact are calculated, the velocities after the impact are obtained using Equations (20) and (21). If transition takes place toward pattern 1 or 2, using the approach proposed in Spanos et al.,[26] Equations (20), (21) and consequently velocities can be expressed as:

$$\begin{cases} J_1\dot{\theta}_1^{-} + J_2\,\dot{\theta}_2^{-} = J_3\,\dot{\theta}_1^{+} + J_4\dot{\theta}_2^{+} \\ J_5\dot{\theta}_1^{-} + J_6\,\dot{\theta}_2^{-} = J_7\,\dot{\theta}_1^{+} + J_8\dot{\theta}_2^{+} \end{cases} \rightarrow \begin{cases} \dot{\theta}_1^{+} = \dfrac{J_1J_8 - J_5J_4}{J_3J_8 - J_7J_4}\,\dot{\theta}_1^{-} + \dfrac{J_2J_8 - J_6J_4}{J_3J_8 - J_7J_4}\dot{\theta}_2^{-} \\ \dot{\theta}_2^{+} = \dfrac{J_1J_7 - J_5J_3}{J_4J_7 - J_6J_3}\,\dot{\theta}_1^{-} + \dfrac{J_2J_7 - J_7J_3}{J_4J_7 - J_6J_3}\dot{\theta}_2^{-} \end{cases} \tag{24}$$

where $J_1$, $J_5$ and $J_2$, $J_6$ are the coefficients of velocities before impact of lower and upper bodies, respectively, $J_3$, $J_7$ and $J_4$, $J_8$ are the coefficients of velocities after impact of lower and upper bodies, respectively.

If the transition, following an impact, happens toward pattern 3, the velocity $\dot{\theta}$ of the monolithic system must be determined. In this case, Equation (20) becomes:

$$J_1\dot{\theta}_1^{-} + J_2\,\dot{\theta}_2^{-} = J_3\,\dot{\theta}^{+} \;\rightarrow\; \dot{\theta}^{+} = \frac{J_1\dot{\theta}_1^{-} + J_2\dot{\theta}_2^{-}}{J_3} \tag{25}$$

If following the impact, the system moves in pattern 4 the velocity $\dot{\theta}_2^{+}$ of the upper body can be determined as

$$J_1\dot{\theta}_1^{-} + J_2\,\dot{\theta}_2^{-} = J_4\,\dot{\theta}_2^{+} \rightarrow\; \dot{\theta}_2^{+} = \frac{J_1\dot{\theta}_1^{-} + J_2\dot{\theta}_2^{-}}{J_4} \tag{26}$$

The $J_i$ coefficients for every impact case are now derived. The impact cases are divided in middle impact cases if the impact occurs between the two bodies, and base impact cases, when the impact occurs between the foundation and the lower body. Pattern changes, due to impact phenomena, are subsequently examined with respect to the positive case only. However, given the symmetry of the system, the coefficients to evaluate the angular velocities after the impact are equal for positive and negative cases.

Following each impact, the system can transit toward two different patterns. These two possible transitions can be divided into two categories: the first one where both bodies are in motion, and the second one that requires the lower body to stop or the system to move monolithically. Following each impact, the angular velocities of the pattern in the first

**TABLE 2** Pattern changes due to impact

| From | Event | To | Kinematic assumption check | | Assumption | To |
|---|---|---|---|---|---|---|
| 1a | $\theta_1 = \theta_2$ | 2a | $\dot{\theta}_1^+ > \dot{\theta}_2^+$ | False → | $\dot{\theta}_1^+ = \dot{\theta}_2^+$ | 3a |
| 2a | $\theta_1 = \theta_2$ | 1a | $\dot{\theta}_1^+ < \dot{\theta}_2^+$ | False → | $\dot{\theta}_1^+ = \dot{\theta}_2^+$ | 3a |
| 4a | $\theta_1 = \theta_2$ | 1b | $\dot{\theta}_1^+ < 0$ | False → | $\dot{\theta}_1^+ = 0$ | 4b |
| 1a | $\theta_1 = 0$ | 2b | $\dot{\theta}_1^+ < 0$ | False → | $\dot{\theta}_1^+ = 0$ | 4a |
| 2a | $\theta_1 = 0$ | 1b | $\dot{\theta}_1^+ < 0$ | False → | $\dot{\theta}_1^+ = 0$ | 4b |
| 3a | $\theta_1 = 0$ | 1b | $\dot{\theta}_1^+ > \dot{\theta}_2^+$ | False → | $\dot{\theta}_1^+ = \dot{\theta}_2^+$ | 3b |

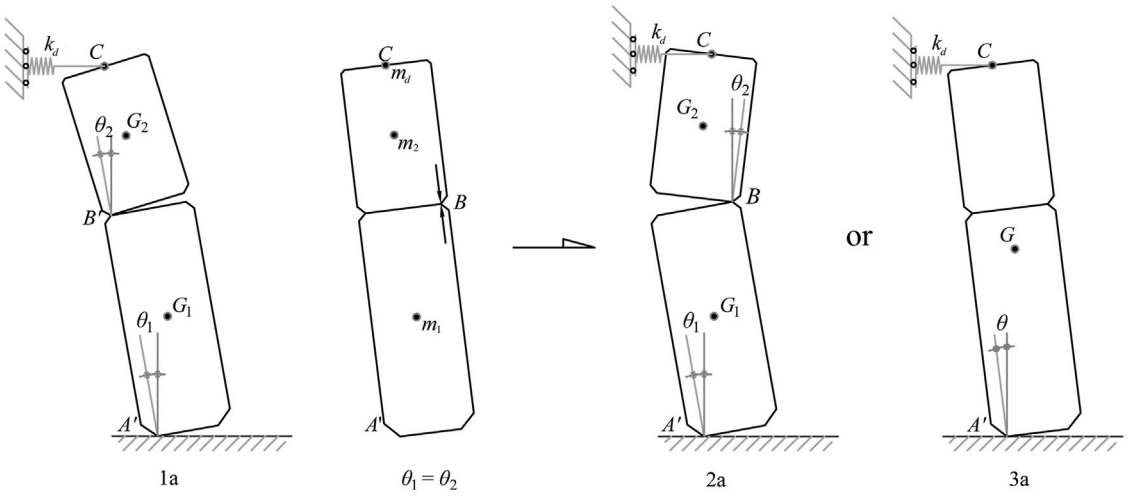


**FIGURE 5** Transition from pattern 1a to 2a or to 3a due to a middle impact

category are calculated. Then, a kinematic check on the angular velocities is performed to investigate if the pattern change involves a compenetration. If the control is not satisfied, a kinematic assumption (that the base block stops or that the system moves monolithically) is introduced and the second possible pattern is considered. All possible positive pattern changes and checks are listed in Table 2.

When the system is moving in pattern 1, both bodies have a positive rotation, but the upper one has a larger rotation than the lower body. If an impact between the two of them occurs, the rotation of the upper body becomes less than that of the lower one and the point of contact between them moves from *B'* to *B*. The $J_i$ coefficients, necessary to evaluate the angular velocities after the impact according to Equation (24), in the case of transition from pattern 1a to 2a (Figure 5), are:

$$
\begin{aligned}
&J_1 = I_{G_1} + b_1\left(b_1A_1 - b_2A_2\right) + h_1\left(2h_2A_4 + h_1A_5\right); \quad J_2 = I_{G_2} + b_1b_2A_2 + 2h_1h_2A_4 + h_2^2A_6\\
&J_3 = I_{G_1} + b_1\left(b_1A_1 + b_2A_2\right) + h_1\left(2h_2A_4 + h_1A_5\right); \quad J_4 = I_{G_2} - b_1b_2A_2 + 2h_1h_2A_4 + h_2^2A_6\\
&J_5 = -\left(b_1 - b_2\right)b_1A_2 + 2h_2^2A_4; \quad J_6 = I_{G_2} - b_2^2A_2 + h_2^2A_6\\
&J_7 = -\left(b_1 + b_2\right)b_2A_2 + 2h_1h_2A_4; \quad J_8 = I_{G_2} + b_2^2A_2 + h_2^2A_6
\end{aligned}
\tag{27}
$$

Following the calculation of the angular velocities after the impact, if the kinematic assumption $\dot{\theta}_1^+ > \dot{\theta}_2^+$ is not respected, the lower and upper bodies are assumed to move with the same angular velocity, $\dot{\theta}_1^+ = \dot{\theta}_2^+$, and the system moves in pattern 3a. As shown in Equation (25), if the transition happens toward pattern 3 only three $J_i$ coefficients are necessary. In the transition from pattern 1a to 3a (Figure 5) the coefficient $J_1$ and $J_2$ are the same as in the previous case, while coefficient $J_3$ is equal to:

$$
J_3 = I_G + b_1^2A_1 + h^2\,A_8 \tag{28}
$$

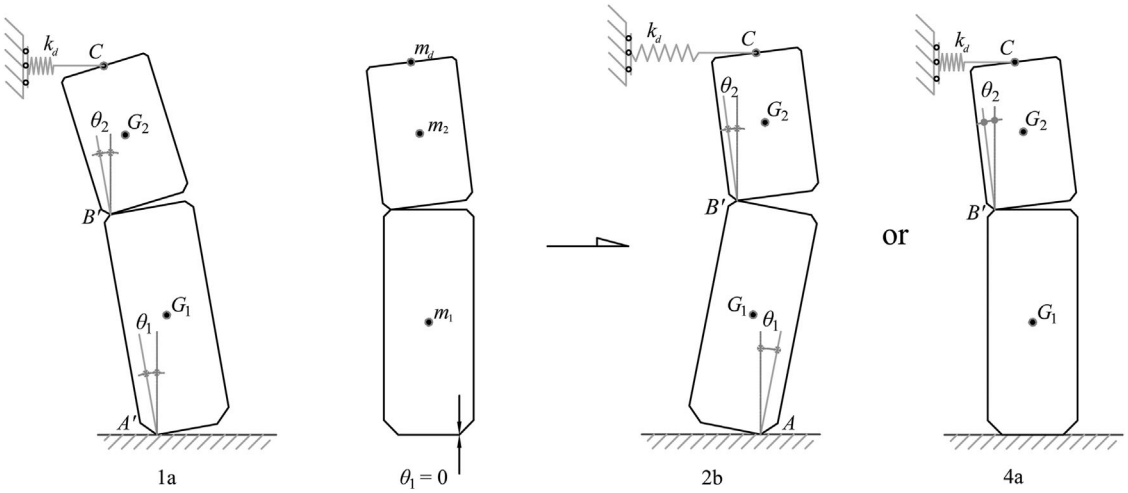


**FIGURE 6** Transition from pattern 1a to 2b or to 4a due to a base impact

During the motion in pattern 1a, if the lower body impacts the foundation its rotation becomes negative and its rotation center moves from $A$' to $A$ (Figure 6). As a result of this impact the system moves to pattern 2b. The new angular velocities are calculated, according to Equation (24), by means of the following coefficients:

$$
\begin{aligned}
J_1 &= I_{G_1} + (2b_2h_1A_2 - b_1h_2A_4 + b_2h_2A_4)\sin|\theta_2| + \left(b_1b_2A_2 + 2h_1h_2A_4 - b_2^2A_2\right)\cos|\theta_2| + b_2^2A_2 - b_1^2A_1 + h_1^2A_5 \\
J_2 &= I_{G_2} + (2b_2h_1A_2 + b_2h_2A_4 + b_1h_2A_4)\sin|\theta_2| + \left(2h_1h_2A_4 - b_1b_2A_2 - b_2^2A_2\right)\cos|\theta_2| - b_2^2A_2 + h_2^2A_6 \\
J_3 &= I_{G_1} + (b_1A_4 + 2b_2h_1A_2 + b_2A_4)\sin|\theta_2| + \left(2h_1h_2A_4 - b_2^2A_2 - b_1b_2A_2\right)\cos|\theta_2| \\
&\quad + b_2(b_2 + 2b_1)A_2 + b_1^2A_1 + h_1^2A_5 \\
J_4 &= I_{G_2} + (2b_2h_1A_2 + b_2h_2A_4 + b_1h_2A_4)\sin|\theta_2| + \left(2h_1h_2A_4 - b_1b_2A_2 - b_2^2A_2\right)\cos|\theta_2| - b_2^2A_2 + h_2^2A_6 \\
J_5 &= (2b_2h_1A_2 + b_2h_2A_4 - b_2b_1A_4)\sin|\theta_2| + (-b_2^2A_2 + b_1b_2A_2 + 2h_1h_2A_4)\cos|\theta_2| \\
J_6 &= I_{G_2} + b_2^2A_2 + h_2^2A_6 \\
J_7 &= (b_1h_2A_4 + 2b_2h_1A_2 + b_2h_2A_4)\sin|\theta_2| + \left(-b_2^2A_2 - b_1b_2A_2 + 2h_1h_2A_4\right)\cos|\theta_2| \,; J_8 = I_{G_2} + b_2^2A_2 + h_2^2A_6
\end{aligned}
\tag{29}
$$

Then, the kinematic assumption $\dot{\theta}_1^+ < 0$ must be checked. If the assumption is not fulfilled, the lower body is assumed at rest and the system moves according to pattern 4a (Figure 6). In this case, according to Equation (26), the velocity of the upper body is computed using the coefficients $J_1$, $J_2$, and $J_4$ which are the same as in Equation (29).

The coefficients to be used in Equation (24) through Equation (26), for all other combinations of pattern changes due to impacts are presented in Appendix C.

## 6 | EVENT STRATEGIES

Once the equations of motion for each pattern are defined and all the possible pattern changes mapped, the motion of the system can be described. A threshold acceleration $\ddot{x}_{g,\text{rest},\,i}$ , also called uplift acceleration,[45–47] must be overcome to trigger the system at rest into motion, and it can be determined for each pattern from the equation of motion setting rotations, velocities, and accelerations of the system equal to zero. Because the spring at the top does not contribute when the system is at rest, it is assumed that motion starts according to pattern 2 or pattern 3, and corresponding threshold accelerations are given in Equation (30). It is worth noting that in the case of $\ddot{x}_{g,\text{rest},2}$, the acceleration is equal to the case of a rigid top

restraints.[11]

$$\ddot{x}_{g,\text{rest},2} = \frac{(g+y_g)\left[b_1 h_2 A_1 + b_2 (h_1+h_2) A_2\right]}{h_1 h_2 (m_1+m_2)};\ \ddot{x}_{g,\text{rest},3} = \frac{(g+y_g)\, b_2 (b_1 A_1 + b_2 A_2 + b_1 m_1)}{b_1 h_2 A_4 + b_2 (2h_1 A_3 + h_2 A_4)} \tag{30}$$

Depending on the lower threshold acceleration between $\ddot{x}_{g,\text{rest},2}$ . and $\ddot{x}_{g,\text{rest},3}$ , the system begins to oscillate in pattern 2 or 3, respectively. In most cases, motion initiation occurs in pattern 3, However, because pattern changes are controlled for each integration step, the system will quickly move to a different configuration if appropriate.

After motion is initiated, the equation of motion for the specific pattern must be integrated. The matrix form used to describe the equations of motion (Equation 6), in addition to being easy to interpret, is also of practical use for numerical implementation in a MATLAB environment. As a first action, it is necessary to reduce the equations of motion to first order general form as in Equation (31).

$$M^*(t\ ;\ \theta_1\ ;\ \theta_2\ )\ \dot{Y}\ (t) = F^*\ \left(t\ ;\ \theta_1\ ;\ \theta_2\ ;\dot{\theta}_1\ ;\ \dot{\theta}_2\ ;\ k_d\ ;\ddot{x}_g;\ \ddot{y}_g\right) \tag{31}$$

where $\mathbf{M}^*$ is the mass matrix,$\dot{\mathbf{Y}}(t)$ the first order derivative vector, and $\mathbf{F}^*$is the vector that contains the rotations as well as the known terms, all of them obtained after the transformation to the first order general form.

The numerical integration is performed with the function "ode45," which implements a Runge–Kutta method with a variable time step. Resorting to this function necessitates the use of an event function. In fact, during each step of the integration specific events may occur: (a) overturning; (b) base impact $\theta_1 = 0$ and middle impact $\theta_1 = \theta_2$; (c) pattern change due to an acceleration exceeding the relevant value. Once the nature of the event is identified, it is necessary to define action strategies. In the case of event (a) the rotation of one body exceeds the critical rotation $\theta_{cr} = \pi/2$, resulting in overturning and the analysis being terminated. If an event (b) is detected, as already-mentioned, Table 2 is applied.

After calculating the post-impact angular velocities, it is always necessary to control if the system stops, even if the ground acceleration time history is not finished yet. An energy control is used for this purpose: the total energy (reduced by the potential energy calculated for system at rest $V_{\text{rest}}$) $E = T + V - V_{\text{rest}}$, must be less than a minimum energy, herein assumed as $E_{\min} = 10^{-6}\ \ T_{\text{cr}}$ (where $T_{\text{cr}}$ is the kinetic energy that provided to the system at rest overturns it). In this case, the system stops its motion until the ground motion final time, $t_{\text{end}}$, is reached or an acceleration large enough to restart the motion is detected.

If the detected event is (c) a pattern change without impact occurs as a result of an acceleration exceeding the threshold value among those provided by Equations (17) and (18) and Appendix B, summarized in Table 1. In this case, it is sufficient to restart with the numerical integration of the new pattern equations of motion. The global solution procedure used is described by the flowchart in Figure 7.

## 7 | NUMERICAL EXEMPLIFICATIONS

In order to exemplify the potential of the model and the event procedure, the response of a specific wall to a given earthquake record is shown. It is assumed: $2b_1 = 2b_2 = 0.40$ m, $2h_1 = 1.75$ m, and $2h_2 = 1.25$ m, consequently the ratio between the height of the lower body and the total height is $\xi = 0.55$.[36] The masonry density is assumed as $\rho = 1800$ kg/m$^3$, the ratio between the mass of the diaphragm and that of the wall is set equal to $\chi = 0.05$, while the diaphragm stiffness is assumed as $k_d = 400$ kN/m. The response is analyzed for an accelerogram (Figure 8) recorded during the Imperial Valley, CA, USA earthquake (Date: 1979-10-15, Station: El Centro Array #7, Record: IVC230).

The system begins its motion in pattern 3a at instant $t = 4.82$ s, when the acceleration reaches the value $\ddot{x}_g = 0.16$ g. The system continues to oscillate until $t = 9.63$ s, when the acceleration becomes less than 0.05 g. Figure 9 shows the rotations of the two bodies and the pattern changes that the system undergoes during motion. Contrary to what frequent in the literature of one DOF rocking systems, the rotations of the two bodies are not normalized with respect to their instability rotations: $\alpha_i = \arctan(b_i/h_i)$, because otherwise the occurrence of the middle impact or of pattern 3, when both bodies have the same rotation, would not be evident anymore.

The response of the system, during its most severe phases, is now examined in detail. After the system has started its motion in pattern 3a, the first configuration change occurs due to a sudden acceleration ($\ddot{x}_g = 0.44$ g at $t = 4.94$ s). The system moves to pattern 2a and the rotations of the two bodies grow considerably (Figure 10A). Subsequently, when

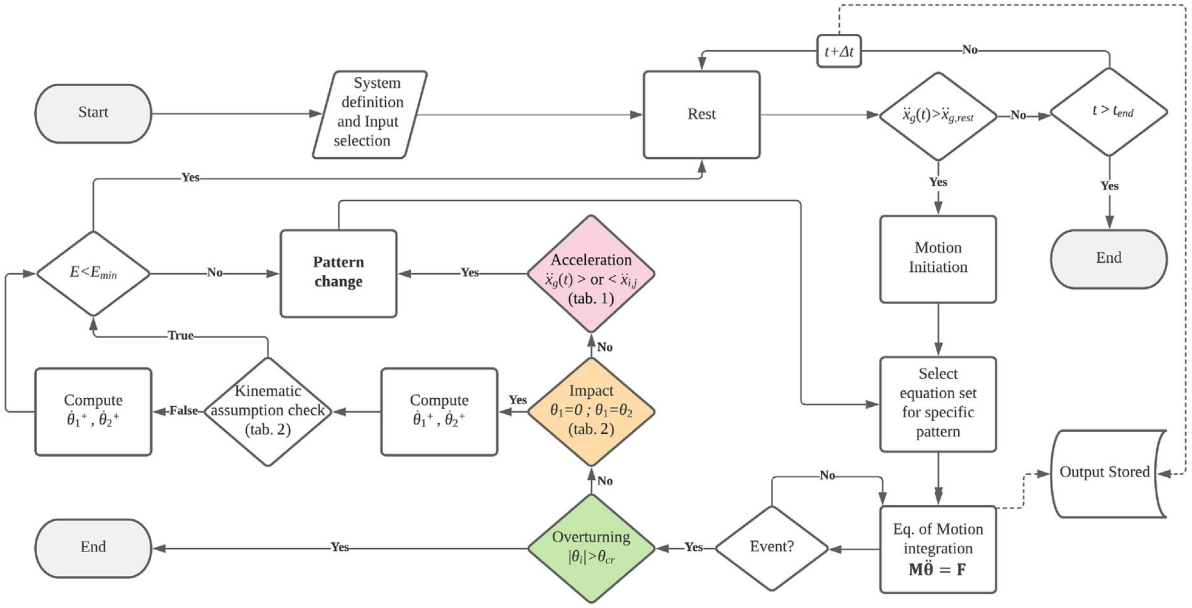


**FIGURE 7** Flowchart of the event strategies

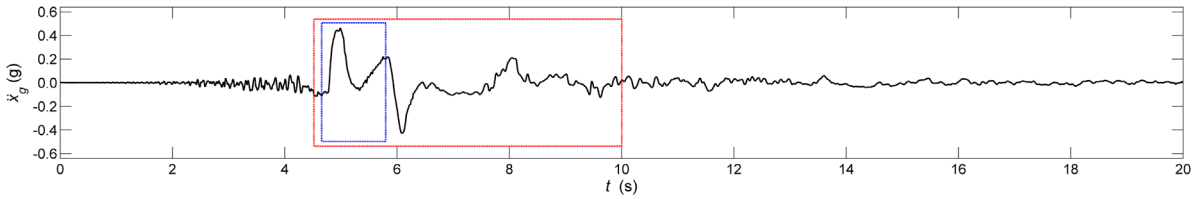


**FIGURE 8** Accelerogram Imperial Valley, CA, USA earthquake. Boxed time windows related to Figure 9 (red) and Figure 11 (blue)

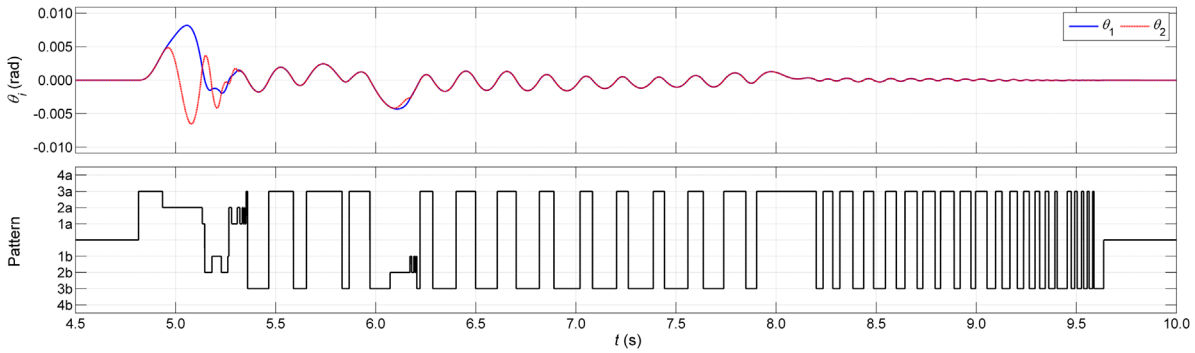


**FIGURE 9** Rotations and pattern vs time. $\alpha = 0.132$; $\alpha_1 = 0.225$; $\alpha_2 = 0.310$ rad

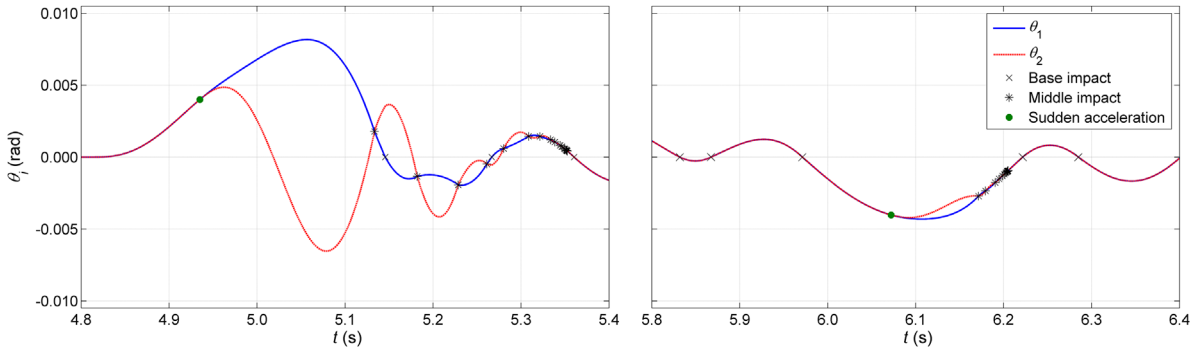


**FIGURE 10** Rotation histories for specific time windows

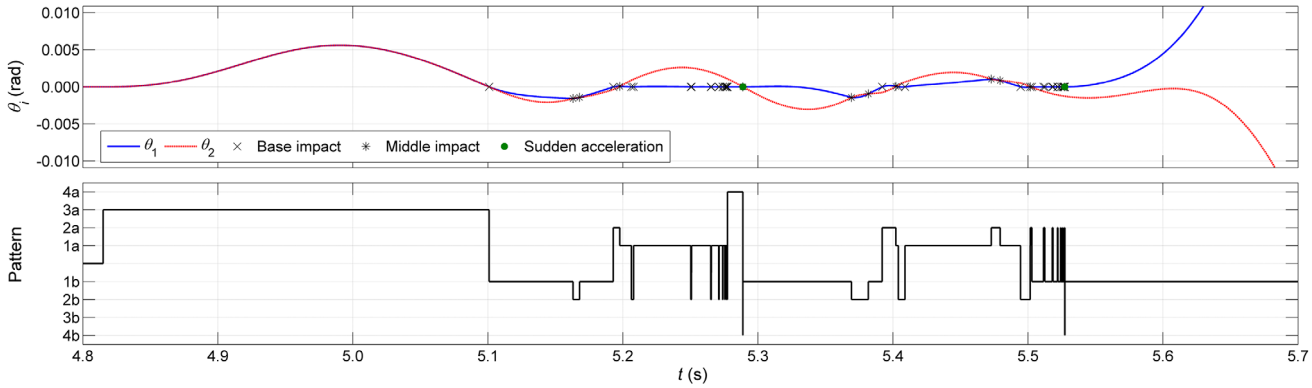


**FIGURE 11** Rotations and pattern versus time, for squat lower body. $\alpha = 0.133$; $\alpha_1 = 0.418$; $\alpha_2 = 0.142$ rad

the acceleration has decreased, the upper body tends to impact several times on the lower one dissipating energy until the system begins to oscillate monolithically in patterns 3a and 3b. Near a second peak, at $t = 6.07$ s, another acceleration causes again the separation of the two bodies (Figure 10B). Once the seismic action reduces its intensity, a series of impacts close to each other occur, dissipating energy until the system returns to oscillating monolithically. In fact, for squat walls, a strong excitation and a stiff diaphragm are necessary to open the intermediate crack.

In Spanos et al.[26] transitions toward pattern 4, due to a base impact, were neglected. In order to capture this possible change, some characteristics of the previous model are modified. The diaphragm properties remained the same of the previous case. The upper body is assumed to be more slender, $2b_2 = 0.30$ m and $2h_2 = 2.10$ m, while the lower body is assumed to be squatter, $2b_1 = 0.40$ m and $2h_1 = 0.90$ m, consequently $\xi = 0.30$. Using the previous accelerogram (Figure 8) the response of the modified system is evaluated (Figure 11). The system starts its motion at $t = 4.81$ s, according to pattern 3a because the combined system is more slender than the upper body alone. Then, at $t = 5.10$ s, the lower body impacts the foundation transitioning from pattern 3a to 1b. Subsequently, after some middle impacts, the lower body loses energy and, because it is very squat, tends to rest. At $t = 5.28$ s, the system impacts the foundation and the pattern changes from 1a to 4a. A similar behavior can be observed at $t = 5.53$ s, when the lower body hits the foundation and the pattern changes from 1b to 4b. Then, while the system is moving in pattern 4b, another acceleration triggers the motion of the lower body, so that system moves in pattern 1b and eventually overturns. Hence, accounting for a transition toward pattern 4 due to a base impact is necessary, specifically for a slender body supported by a squat one. Neglecting such a pattern change may lead to underestimate overturning.

## 8 | RESPONSE TO SINE PULSE EXCITATION

In order to further describe the behavior of the system, a sine pulse analysis is conducted. Although, a sine pulse is usually rather far from a real earthquake ground motion, it can still be powerful to understand the dynamics of the wall under consideration.[48,49] First of all, the equation of motion of pattern 3 is linearized as follows:

$$\ddot{\theta} = \mathrm{S}_\theta \, P^2 \, (|\theta| - B) \tag{32}$$

where

$$P^2 = \frac{h\,(A_7 g + 4hk_d)}{A_1 b_1^2 + A_8 h^2 + I_G}; \; D = \frac{A_1 b_1 g}{h\,(A_7 g + 4hk_d)} \tag{33}$$

For a monolithic wall restrained by an elastic spring of $k_d$ stiffness, $P$ is the equivalent of the frequency parameter of Housner's inverted pendulum,[27] while $D$ is the equivalent of the rotation capacity: if no diaphragm is present, $D = b_1/h$, which is the linearization of $\alpha$. Parameter $P$ in Equation (33) will be used in the following to perform a first normalization of the circular frequency, $\omega_p$, of the sine pulse, while its amplitude, $a_p$, will be made non-dimensional dividing it by

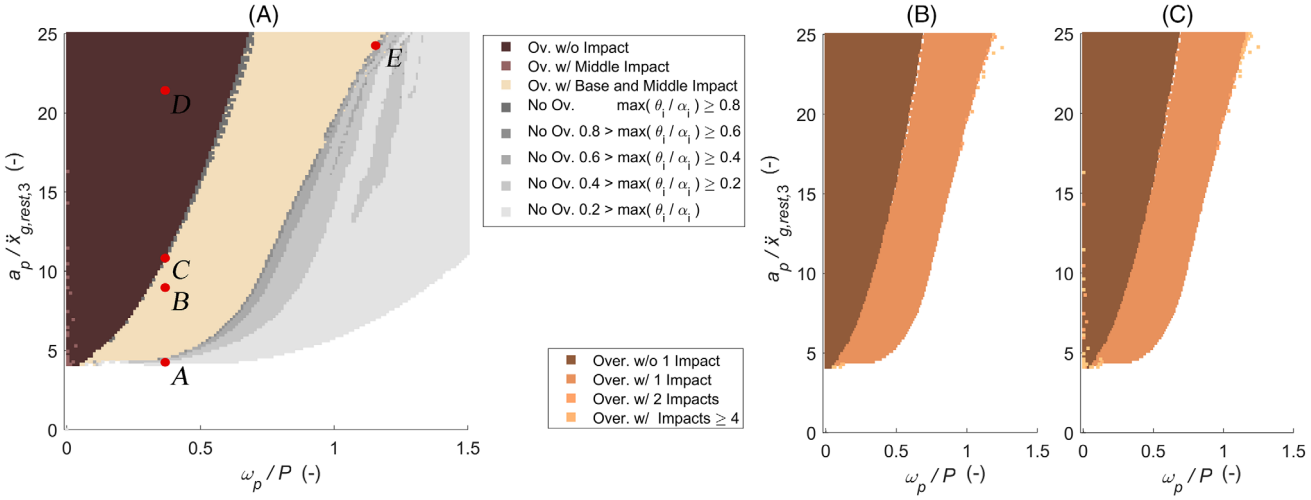


**FIGURE 12** Rocking spectra for a two-bodies vertical spanning wall elastically restrained at the top: (A) overturning or maximum rotation, (B) number of base impacts, (C) number of middle impacts

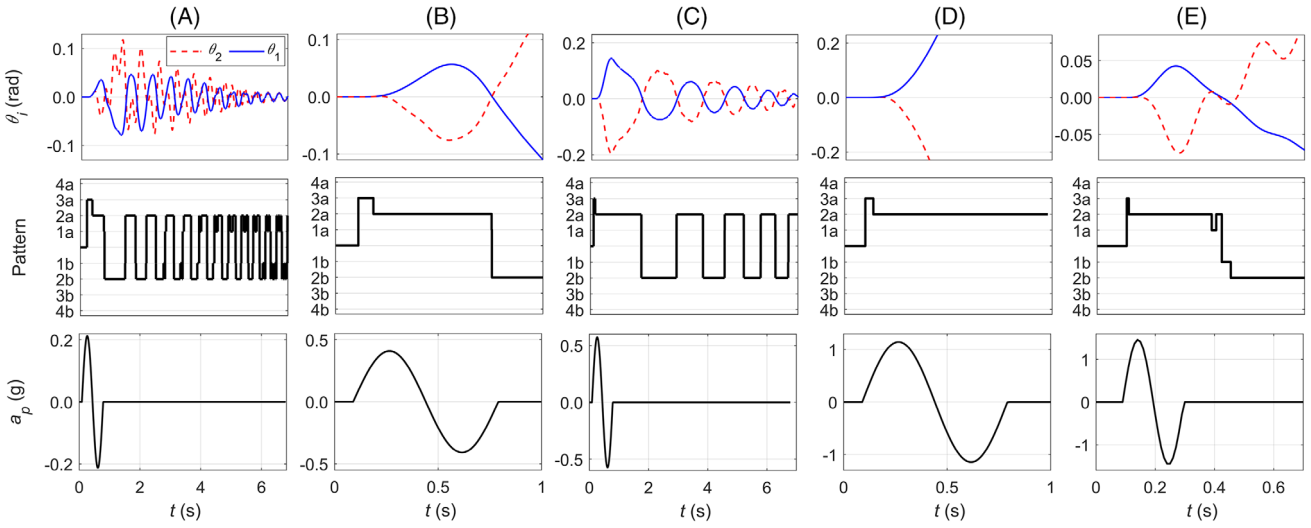


**FIGURE 13** Rotation, pattern, excitation versus time, for A, B, C, D, E points in Figure 12

the threshold acceleration in Equation (30). However, it should be considered that during its dynamic response the wall elastically restrained at the top can change pattern and therefore these parameters are not fully consistent anymore.

Considering for instance the example in Derakhshan et al.,[14] the following wall characteristics can be assumed: $2b_1 = 2b_2 = 0.23$ m, $2h = 4.1$ m, $\xi = 0.57$, and $\rho = 1800$ kg/m$^3$. Additionally, it is postulated that $\chi = 0.05$ and $k_d = 400$ kN/m. The maximum response for non-dimensional sine pulse parameters is presented in Figure 12A, reporting the overturning of the wall or its maximum normalized rotation for 22,500 time history analyses. It is possible to recognize two clearly separated regions, corresponding to an overturning without impact and to an overturning after one or more impacts. Impacts can involve the middle crack alone or both the middle and the base cracks, while overturning with base impact alone never takes place. Hence, an important difference with respect to two stacked blocks unrestrained at the top occurs, because in such case overturning with base impact alone is rather frequent.[31] Additionally, two significant changes are present in comparison to Housner's monolithic inverted pendulum rocking spectra. First of all, for Housner's pendulum at most one impact can occur before overturning,[50] while the response in Figure 12B, C is characterized by several impacts before the collapse, as will be shown in the following with a sample time history. Additionally, again for Housner's

pendulum there are non-dimensional frequencies for which overturning occurs only without impacts, whatever the non-dimensional amplitude. This behavior cannot be observed in Figure 12A, wherein (for equal frequency) an overturning with impacts always occurs for an amplitude smaller than that needed to obtain an overturning without impacts. Finally, the comparison with a wall having the same geometry but $k_d = 4000$ kN/m as in ref. [51] not presented for the sake of conciseness, shows similar trends and, for equal dimensional input, a 4% reduction of the overturning frequency.

Sample time histories are shown in Figure 13 increasing the amplitude of the sine pulse for an equal circular frequency (points A–D in Figure 12). The sequence of no overturning, overturning, no overturning, overturning is clearly evident. Overturning occurs in all cases in pattern 2 and this behavior is systematic, as highlighted by a specific plot not shown for the sake of conciseness. The time history E in Figure 13, related to point E in Figure 12, shows that multiple impacts (three in the middle and one at the base) may occur before overturning as a consequence of multiple pattern changes due to wall kinematic conditions in terms of rotations and velocities, as well as impulsive forces. In conclusion the sine pulse response of the two-bodies vertical spanning wall elastically restrained at the top is similar but more articulated than that of Housner's inverted pendulum.

## 9 | CONCLUSIONS

The dynamic response of two stacked rigid bodies elastically restrained at the top is studied in this paper. Friction is assumed large enough to prevent any sliding, impacts are assumed to be punctual, bodies are assumed to rock about the indented corners. The dynamic behavior of the system, despite the simplicity of the model, turns out to be complex. A set of two strongly non-linear second order coupled differential equations for four distinct patterns, each including a symmetric case, are derived using a Lagrangian method. Kinematic criteria are developed for all possible pattern transitions. A pattern transition can take place due to an impact, either between the lower body and the foundation or between the two bodies, with a consequent loss of energy. Pattern transitions are also found to occur without impact as a result of a strong ground excitation. In this case, the transition occurs without energy dissipation and calculating overturning and resisting moments delivers the corresponding pattern change controlling equations.

The event strategies employed in the development of the computer program in this work are then described. While the integration of the equation of motion for the specific pattern is being performed, the numerical model must be capable of capturing all possible phenomena, such as pattern changes. To this purpose the event function in MATLAB environment proved to be essential. Some numerical exemplifications are performed to demonstrate the potential of the model and of the event procedure. The dynamic response of specific walls to a given earthquake record confirms the strong nonlinearity of the numerical model, demonstrating how the motion is characterized by several pattern changes with and without impacts. Then, for systems in which the upper body is slender, the importance of considering all possible transitions between patterns, which were neglected in previous works, is demonstrated.

Finally, the response of the system to a sine pulse excitation revealed how the two-bodies vertical spanning wall, elastically restrained at the top, has a similar but more complex response compared to Housner's inverted pendulum. Overturning is frequently preceded by multiple impacts and always occurs in pattern 2.

The developed model can be used for extensive parametric analyses, accounting for different wall and diaphragms properties, as well as record suites. Moreover, several additional studies are possible. The model could account for diaphragm viscous damping. Internal forces at connections could be computed and compared to reasonable strength values to determine whether the diaphragm is truly capable of restraining the wall. Finally, a model starting with a monolithic wall and cracking when assigned masonry tensile strength is exceeded could be implemented.

### ACKNOWLEDGEMENTS

This work was partially carried out under the research program SISTINA (SIStemi Tradizionali e INnovativi di tirantatura delle Architetture storiche) funded by Sapienza University of Rome and under the research program "Dipartimento di Protezione Civile – Consorzio RELUIS." The opinions expressed in this publication are those of the authors and are not necessarily endorsed by the funding bodies.

Open Access Funding provided by Universita degli Studi di Roma La Sapienza within the CRUI-CARE Agreement.

### DATA AVAILABILITY STATEMENT

Data sharing not applicable to this article as no datasets were generated or analyzed during the current study.

## ORCID

*Giacomo Destro Bisol* https://orcid.org/0000-0002-1266-9065
*Omar AlShawa* https://orcid.org/0000-0001-7905-5482
*Luigi Sorrentino* https://orcid.org/0000-0003-1652-942X


## REFERENCES


1. Lourenço PB, Mendes N, Ramos LF, Oliveira DV. Analysis of masonry structures without box behavior. *Int J Architect Herit*. 2011;5(4–5):369–382.
2. de Felice G, Liberatore D, De Santis S, et al. Seismic behaviour of rubble masonry: shake table test and numerical modelling. *Earthq Eng Struct Dyn*. 2022;51(5):1245–1266.
3. Bruneau M. State-of-the-art report on seismic performance of unreinforced masonry buildings. *J Struct Eng*. 1994;120(1):230–251.
4. Moon L, Dizhur D, Senaldi I, et al. The demise of the URM building stock in Christchurch during the 2010–2011 Canterbury earthquake sequence. *Earthq Spectra*. 2014;30(1):253–276.
5. Penna A, Morandi P, Rota M, Manzini CF, Da Porto F, Magenes G. Performance of masonry buildings during the Emilia 2012 earthquake. *Bull Earthq Eng*. 2014;12(5):2255–2273.
6. Giuffrè A. A mechanical model for statics and dynamics of historical masonry buildings. In: *Protection of the Architectural Heritage Against Earthquakes, V. Petrini and M. Save eds.* Springer; 1996.
7. Baggio C, Masiani R. Dynamic behaviour of historical masonry. Proceedings of the 9th International *Brick Block Masonry Conference*. 1991;1:473–480.
8. Doherty K, Griffith MC, Lam N, Wilson J. Displacement-based seismic analysis for out-of-plane bending of unreinforced masonry walls. *Earthq Eng Struct Dyn*. 2002;31(4):833–850.
9. Lam NTK, Griffith M, Wilson J, Doherty K. Time–history analysis of URM walls in out-of-plane flexure. *Eng Struct*. 2003;25(6):743–754.
10. Griffith MC, Lam NTK, Wilson JL, Doherty K. Experimental investigation of unreinforced brick masonry walls in flexure. *J Struct Eng*. 2004;130(3):423–432.
11. Sorrentino L, Masiani R, Griffith MC. The vertical spanning strip wall as a coupled rocking rigid body assembly. *Struct Eng Mech*. 2008;29(4):433–454.
12. Wilhelm M, Mojsilović N, Dazio A. Out-of-plane shaking table tests on unreinforced masonry walls. Paper presented at: Proceedings 10th North American Masonry Conference; 2007; St. Louis, MO, USA, 671–682.
13. Meisl CS, Elwood KJ, Ventura CE. Shake table tests on the out-of-plane response of unreinforced masonry walls. *Can J Civ Eng*. 2007;34(11):1381–1392.
14. Derakhshan H, Griffith MC, Ingham JM. Airbag testing of multi-leaf unreinforced masonry walls subjected to one-way bending. *Eng Struct*. 2013;57:512–522.
15. DeJong MJ, Dimitrakopoulos EG. Dynamically equivalent rocking structures. *Earthq Eng Struct Dyn*. 2014;43(10):1543–1563.
16. Godio M, Beyer K. Evaluation of force-based and displacement-based out-of-plane seismic assessment methods for unreinforced masonry walls through refined model simulations. *Earthq Eng Struct Dyn*. 2019;48(4):454–475.
17. Meriggi P, de Felice G, De Santis S, Gobbin F, Mordanova A, Pantò B. Distinct element modelling of masonry walls under out-of-plane seismic loading. *Int J Archit Herit*. 2019;13(7):1110–1123.
18. Galvez F, Sorrentino L, Dizhur D, Ingham JM. Using DEM to investigate boundary conditions for rocking URM facades subjected to earthquake motion. *J Struct Eng*. 2021;147(11):04021191.
19. Galvez F, Sorrentino L, Dizhur D, Ingham J. Damping considerations for rocking block dynamics using the discrete element method. *Earthq Eng Struct Dyn*. 2022;51:935–957
20. Noor-E-Khuda S, Dhanasekar M, Thambiratnam DP. An explicit finite element modelling method for masonry walls under out-of-plane loading. *Eng Struct*. 2016;113:103–120.
21. Malomo D, Pinho R, Penna A. Numerical modelling of the out-of-plane response of full-scale brick masonry prototypes subjected to incremental dynamic shake-table tests. *Eng Struct*. 2020;209:110298.
22. Malomo D, DeJong MJ. A Macro-Distinct Element Model (M-DEM) for out-of-plane analysis of unreinforced masonry structures. *Eng Struct*. 2021;244:112754.
23. Pantò B, Cannizzaro F, Caliò I, Lourenço PB. Numerical and experimental validation of a 3D macro-model for the in-plane and out-of-plane behavior of unreinforced masonry walls. *Int J Archit Herit*. 2017;11(7):946–964.
24. Casapulla C, Giresini L, Lourenço PB. Rocking and kinematic approaches for rigid block analysis of masonry walls: state of the art and recent developments. *Buildings*. 2017;7(3):69.
25. Psycharis IN. Dynamic behaviour of rocking two-block assemblies. *Earthq Eng Struct Dyn*. 1990;19(4):555–575.
26. Spanos PD, Roussis PC, Politis NPA. Dynamic analysis of stacked rigid blocks. *Soil Dyn Earthq Eng*. 2001;21(7):559–578.
27. Housner GW. The behavior of inverted pendulum structures during earthquakes. *Bull Seismol Soc Am*. 1963;53(2):403–417.
28. Kounadis AN, Papadopoulos GJ, Cotsovos DM. Overturning instability of a two-rigid block system under ground excitation. *ZAMM-J Appl Math Mech/Z Angew Math Mech*. 2012;92(7):536–557.
29. Papaloizou L, Komodromos P. Investigating the seismic response of ancient multi-drum colonnades with two rows of columns using an object-oriented designed software. *Adv Eng Software*. 2012;44(1):136–149.

30. Ishiyama Y. Motions of rigid bodies and criteria for overturning by earthquake excitations. *Earthq Eng Struct Dyn*. 1982;10(5):635–650.
31. Chatzis MN, García Espinosa M, Needham C, Williams MS. Energy loss in systems of stacked rocking bodies. *J Eng Mech*. 2018;144(7):04018044.
32. ABK. Methodology for Mitigation of Seismic Hazards in Existing Unreinforced Masonry Buildings: Wall-testing, Out-of-plane. Technical Report ABK-TR-04, ABK, A Joint Venture of Agbabian Associates S.B. Barnes and Associates, and Kariotis and Associates, El, 198, The Corporation; 1981.
33. Simsir CC, Consultants W, Aschheim M, Abrams D. Out-of-plane dynamic response of unreinforced masonry bearing walls attached to flexible diaphragms. Paper presented at: Proceedings 13th World Conference on Earthquake Engineering, Paper No. 2045, Vancouver, B.C.; 2004.
34. Derakhshan H, Griffith MC, Ingham JM. Out-of-plane behavior of one-way spanning unreinforced masonry walls. *J Eng Mech*. 2013;139(4):409–417.
35. Gabellieri R, Landi L, Diotallevi PP. A 2-DOF model for the dynamic analysis of unreinforced masonry walls in out-of-plane bending. Paper presented at: Proceedings 4th ECCOMAS Thematic Conference on Computational Methods in Structural Dynamics and Earthquake Engineering; 2013; Kos Island, Greece.
36. Penner O, Elwood KJ. Out-of-plane dynamic stability of unreinforced masonry walls in one-way bending: shake table testing. *Earthq Spectra*. 2016;32(3):1675–1697.
37. Landi L, Gabellieri R, Diotallevi PP. A model for the out-of-plane dynamic analysis of unreinforced masonry walls in buildings with flexible diaphragms. *Soil Dyn Earthq Eng*. 2015;79:211–222.
38. Derakhshan H, Griffith MC, Ingham JM. Out-of-plane seismic response of vertically spanning URM walls connected to flexible diaphragms. *Earthq Eng Struct Dyn*. 2015;45(4):563–580.
39. Humar J. *Dynamics of Structures*. Prentice-Hall; 1990.
40. Meirovitch L. *Computational Methods in Structural Dynamics*. Sijthoff and Noordhoff; 1980.
41. D'Ayala D, Shi Y. Modeling masonry historic buildings by multi-body dynamics. *Int J Archit Herit*. 2011;5(4-5):483–512.
42. Meriam JL, Kraige LG. *Engineering Mechanics Dynamics*. John Wiley & Sons; 1987.
43. Rao CL, Narayanamurthy V, Simha KRY. *Applied Impact Mechanics*. John Wiley & Sons; 2016.
44. Stronge WJ. *Impact Mechanics*. Cambridge University Press; 2004.
45. Apostolou M, Gazetas G, Garini E. Seismic response of slender rigid structures with foundation uplifting. *Soil Dyn Earthq Eng*. 2007;27(7):642–654.
46. Bachmann JA, Vassiliou MF, Stojadinovic B. Rolling and rocking of rigid uplifting structures. *Earthq Eng Struct Dyn*. 2019;48(14):1556–1574.
47. Alexakis H, Makris N. Minimum uplift horizontal acceleration of the single-nave barrel vault and the rocking frame. *ISSMGE Int J Geoeng Case Histories*. 2018;4(4):275–288.
48. Anooshehpoor A, Heaton TH, Shi B, Brune JN. Estimates of the ground accelerations at Point Reyes Station during the 1906 San Francisco earthquake. *Bull Seismol Soc Am*. 1999;89(4):845–853.
49. Zhang J, Makris N. Rocking response of free-standing blocks under cycloidal pulses. *J Eng Mech*. 2001;127(5):473–483.
50. Dimitrakopoulos EG, DeJong MJ. Revisiting the rocking block: closed-form solutions and similarity laws. *Proc R Soc A: Math Phys Eng Sci*. 2012;468(2144):2294–2318.
51. De Santis S, AlShawa O, de Felice G, et al. Low-impact techniques for seismic strengthening fair faced masonry walls. *Constr Build Mater*. 2021;307:124962.

**How to cite this article:** Prajapati S, Destro Bisol G, AlShawa O, Sorrentino L. Non-linear dynamic model of a two-bodies vertical spanning wall elastically restrained at the top. *Earthquake Engng Struct Dyn*. 2022;51:2627–2647. https://doi.org/10.1002/eqe.3692

## APPENDIX A: EQUATIONS OF MOTION

In this Appendix, the components of the matrix equations of motion (Equation 6) of patterns 2, 3, and 4 are presented (Figure 2).

| | Pattern 2 | Pattern 3 | Pattern 4 |
|---|---|---|---|
| Kinematic configuration | $\theta_1 > 0$ and $\theta_2 < \theta_1$ or $\theta_1 < 0$ and $\theta_2 > \theta_1$ | $\theta_2 = \theta_1 = \theta$ | $\theta_1 = 0$ |
| $M_{11}$ | $I_{G_1} + b_1^2 A_1 + b_2(2b_1 + b_2)A_2 + h_1^2 A_5$ | $I_G + b_1^2 A_1 + h^2\ A_8$ | NA |
| $M_{22}$ | $I_{G_2} + b_2^2 A_2 + h_2^2 A_6$ | NA | $I_{G_2} + b_2^2 A_2 + h_2^2 A_6$ |
| $M_{12} = M_{21}$ | $S_\theta[(b_1 + b_2)h_2 A_4 + 2h_1 b_2 A_2]\sin(\theta_1 - \theta_2)$ $-[(b_1 + b_2)b_2 A_2 - 2h_1 h_2 A_4]\cos(\theta_1 - \theta_2)$ | NA | NA |
| $F_1$ | $\{[b_2(b_1 + b_2)A_2 - 2h_1 h_2 A_4]\sin(\theta_1 - \theta_2)$ $+ S_\theta[2h_1 b_2 A_2 + h_2(b_1 + b_2)A_4]\cos(\theta_1 - \theta_2)\}$ $\dot{\theta}_2 - [(b_1 + b_2)\sin\theta_1 + S_{\theta_1} 2h_1 \cos\theta_1]$ $[b_1(1 - \cos\theta_1) + b_2(\cos\theta_2 - \cos\theta_1)$ $+S_\theta 2h_1 \sin\theta_1 + S_\theta h_2 \sin\theta_2]$ $k_d + [S_\theta(b_1 A_1 + b_2 A_2)\sin\theta_1 + h_1 A_3 \cos\theta_1]$ $\ddot{x}_g - [S_\theta(b_1 A_1 + b_2 A_2)\cos\theta_1 - h_1 A_3 \sin\theta_1]$ $(g + \ddot{y}_g)$ | $[b_1^2(\cos\theta - 1) - S_\theta 2b_1 h(\cos\theta$ $- \cos 2\theta) + 2h^2 \sin 2\theta]$ $k_d + (S_\theta b_1 A_1 \sin\theta + hA_7 \cos\theta)$ $\ddot{x}_g - (S_\theta b_1 A_1 \cos\theta - hA_7 \sin\theta)$ $(g + \ddot{y}_g)$ | NA |
| | $\{[-b_2(b_1 + b_2)A_2 + 2h_1 h_2 A_4]\sin(\theta_1 - \theta_2)$ $-S_\theta[2h_1 b_2 A_2 + h_2(b_1 + b_2)A_4]\cos(\theta_1 - \theta_2)\}$ $\dot{\theta}_1 + (b_2 \sin\theta_2 - S_{\theta_1} 2h_2 \cos\theta_2)$ | | $[b_2^2(\cos\theta_2 - 1)\sin\theta_2$ $-S_\theta 2b_2 h_2(\cos\theta_2 - \cos 2\theta_2)$ |
| $F_2$ | $[b_1(1 - \cos\theta_1) + b_2(\cos\theta_2 - \cos\theta_1)$ $+S_\theta 2h_1 \sin\theta_1 + S_\theta h_2 \sin\theta_2]$ $k_d - (S_\theta b_2 A_2 \sin\theta_2 - h_2 A_4 \cos\theta_2)$ $\ddot{x}_g + (S_\theta b_2 A_2 \cos\theta_2 + h_2 A_4 \sin\theta_2)(g + \ddot{y}_g)$ | NA | $+2h_2^2 \sin 2\theta_2]k_d + (S_\theta b_2 A_2 \sin\theta_2$ $+h_2 A_4 \cos\theta_2)\ddot{x}_g - (S_\theta b_2 A_2 \cos\theta_2$ $-h_2 A_4 \sin\theta_2)(g + \ddot{y}_g)$ |

where $I_G$ is the polar inertia moment about the center of mass of the whole wall. NA, not available.

## APPENDIX B: PATTERN CHANGE DUE TO ACCELERATIONS

In this Appendix, the accelerations involving a pattern change for the system moving according to pattern 4a or 4b are presented (Figure B.1), as summarized in Table 1.

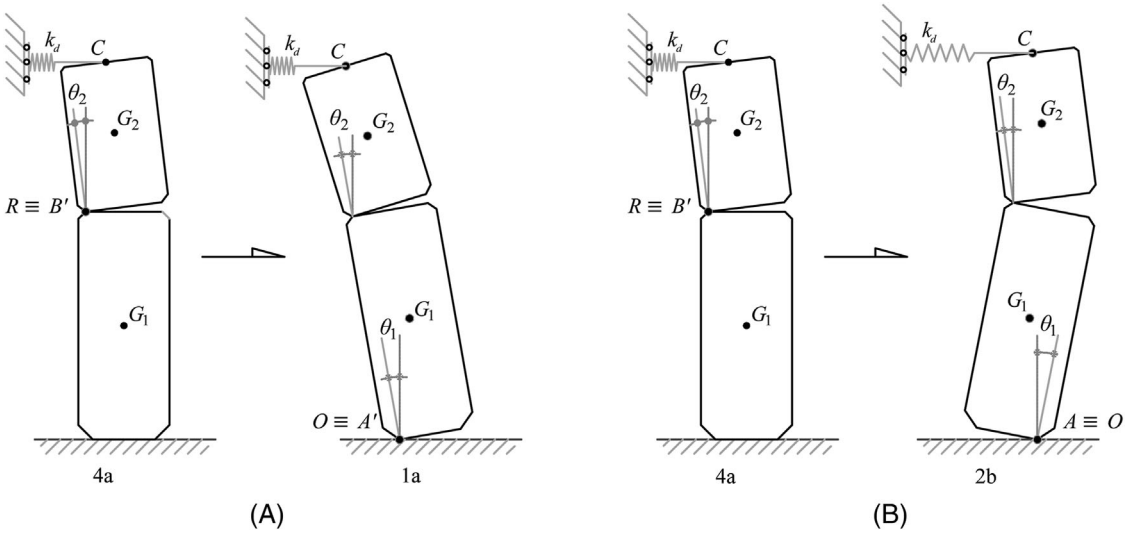


**FIGURE B.1** Transition: (A) from pattern 4a to pattern 1a; (B) from pattern 4a to pattern 2b

| | |
|---|---|
| Pattern change | $\ddot{x}_{4,j}$ $\frac{1}{h_1A_3 + S_\theta b_2A_2 \sin\theta_2 + h_2A_4 \cos\theta_2} \left\{ \begin{bmatrix} I_{G_2} + S_\theta(b_2 - b_1)h_2A_4 \sin\theta_2 + h_2^2A_6 + b_1b_2A_2 \cos\theta_2 \\ +b_2^2A_2(1 - \cos\theta_2) + 2h_1(S_\theta b_2A_2 \sin\theta_2 + h_2A_4 \cos\theta_2) \end{bmatrix} \right.$ |
| From 4 to 1 | $\ddot{\theta}_2 + [(b_2 - b_1)b_2A_2 \sin\theta_2 + S_\theta(b_2 - b_1)h_2A_4 \cos\theta_2 + S_\theta 2h_1b_2A_2 \cos\theta_2 - 2h_1h_2A_4 \sin\theta_2]$<br>$\dot{\theta}_2^2 + [2 \sin\frac{\theta_2}{2}(S_\theta 2h_2 \cos\frac{\theta_2}{2} + b_2 \sin\frac{\theta_2}{2})(2h_1 + 2h_2 \cos\theta_2 + S_\theta b_2 \sin\theta_2)]$<br>$k_d - S_\theta[b_2A_2 - b_1A_1 + S_\theta h_2A_4 \sin\theta_2 - b_2A_2 \cos\theta_2](g + \ddot{y}_g)\}$ |
| From 4 to 2 | $\frac{1}{h_1A_3 + S_\theta b_2A_2 \sin\theta_2 + h_2A_4 \cos\theta_2} \left\{ \begin{bmatrix} I_{G_2} + h_2^2A_6 + b_2^2A_2(1 - \cos\theta_2) + (2h_1h_2A_4 - b_1b_2A_2)\cos\theta_2 \\ +S_\theta 2h_1b_2A_2 \sin\theta_2 + S_\theta(b_1 + b_2)h_2A_4 \sin\theta_2 \end{bmatrix} \right.$<br>$\ddot{\theta}_2 + [(b_1 + b_2)b_2A_2 \sin\theta_2 + S_\theta(b_1 + b_2)h_2A_4 \cos\theta_2 + 2h_1(S_\theta b_2A_2 \cos\theta_2 - h_2A_4 \sin\theta_2)]$<br>$\dot{\theta}_2^2 + [2b_2h_1(1 - \cos\theta_2) - 2b_2h_2(\cos 2\theta_2 - \cos\theta_2) + S_\theta 4h_1h_2 \sin\theta_2 + S_\theta 4h_2^2 \cos 2\theta_2 \sin\theta_2 + S_\theta b_2^2(1 - \cos 2\theta_2)\sin\theta_2]$<br>$k_d - S_\theta[b_1A_1 + b_2A_2 + S_\theta h_2A_4 \sin\theta_2 - b_2A_2 \cos\theta_2](g + \ddot{y}_g)\}$ |

## APPENDIX C: PATTERN CHANGE DUE TO IMPACTS

In this Appendix, the coefficients to be used in Equation (24) to Equation (26) for all other combinations of pattern change due to impacts are presented (Figures C.1–C.4). If an impact has occurred the system can transit toward two different patterns. One of these two patterns is assumed and the angular velocities after the impact are computed accordingly. Then, the kinematic-assumption check in Table 2 is performed and, if it is satisfied, the relevant equations of motion are integrated. If the check is not satisfied, the second pattern is assumed, the angular velocities are computed accordingly, and the corresponding equations of motion are integrated.

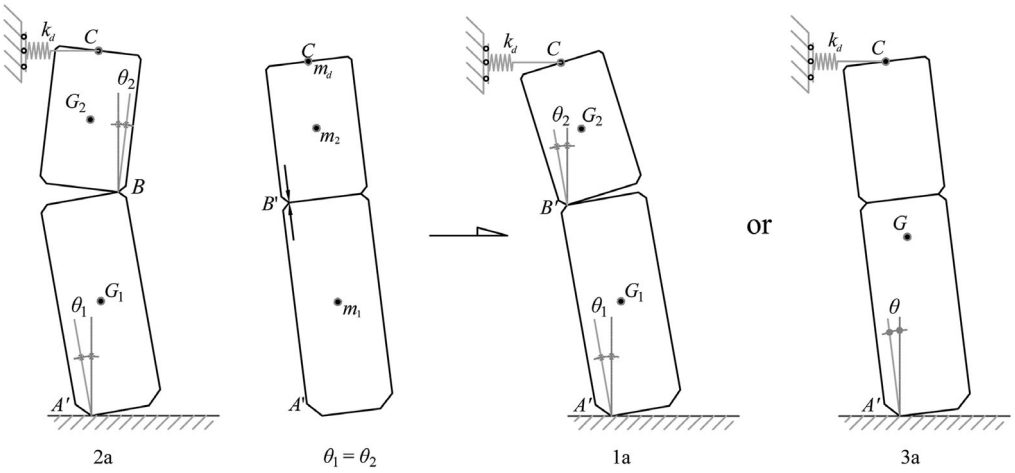


**FIGURE C.1** Transition from pattern 2a to 1a or to 3a due to a middle impact

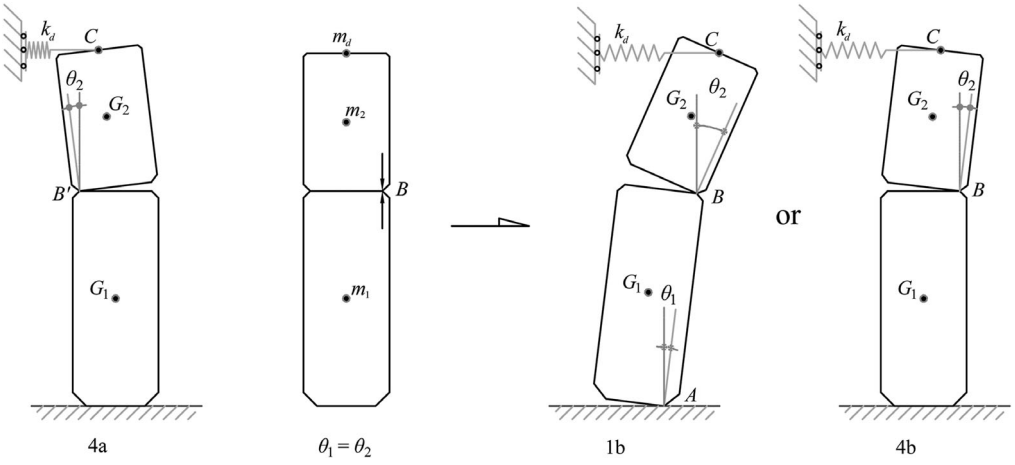


**FIGURE C.2** Transition from pattern 4a to 1b or to 4b due to a middle impact

**FIGURE C.3** Transition from pattern 2a to 1b or to 4b due to a base impact

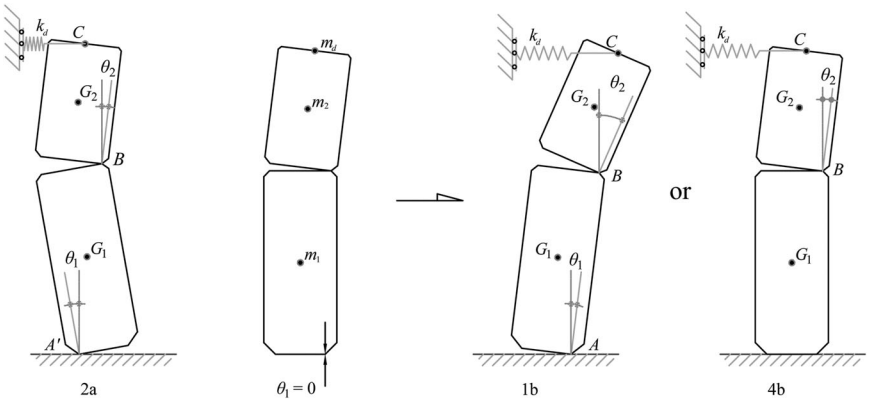


**FIGURE C.4** Transition from pattern 3a to 1b or to 3b due to a base impact

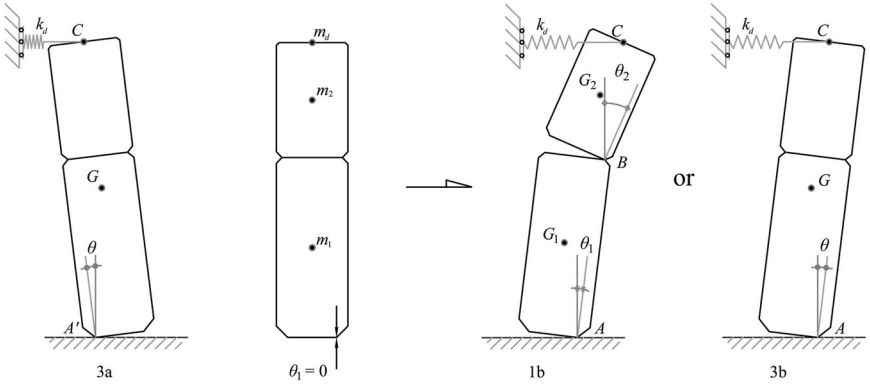


| | Middle impact | | Base impact | |
|---|---|---|---|---|
| | From 2a to 1a | From 4a to 1b | From 2a to 1b | From 3a to 1b |
| | Equation (24) | Equation (24) | Equation (24) | Equation (24) |
| $J_1$ | $I_{G_1} + b_1(b_1A_1 + b_2A_2) + h_1(2h_2A_4 + h_1A_5)$ | $I_{G_1} + h_1(2h_2A_4 + h_1A_5) + b_1(b_1A_1 + b_2A_2)$ | $I_{G_1} - b_2^2A_2 - b_1^2A_1 + h_1^2A_5 - (b_1h_2A_4 + 2h_1b_2A_2 + b_2h_2A_4)\sin\lvert\theta_2\rvert + (2h_1h_2A_4 - b_1b_2A_2 - b_2^2A_2)\cos\lvert\theta_2\rvert$ | $I_G - b_1^2A_1 + h^2A_8$ |
| $J_2$ | $I_{G_2} - b_1b_2A_2 + 2h_1h_2A_4 + h_2^2A_6$ | $I_{G_2} - b_1b_2A_2 + 2h_1h_2A_4 + h_2^2A_6$ | $I_{G_2} - b_2^2A_2 + h_2^2A_6 - (2b_2h_1A_2 + b_2h_2A_4 - b_1h_2A_4)\sin\lvert\theta_2\rvert + (2h_1h_2A_4 + b_1b_2A_2 - b_2^2A_2)\cos\lvert\theta_2\rvert$ | 0 |
| $J_3$ | $I_{G_1} + h_1(2h_2A_4 + h_1A_5) + b_1(b_1A_1 - b_2A_2)$ | $I_G + b_1^2A_1 + h^2\,A_8$ | $I_{G_1} + b_2^2A_2 - 2b_1b_2A_2 + b_1^2A_1 + h_1^2A_5 + (b_1h_2A_4 - 2h_1b_2A_2 - b_2h_2A_4)\sin\lvert\theta_2\rvert + (b_1b_2A_2 + 2h_1h_2A_4 - b_2^2A_2)\cos\lvert\theta_2\rvert$ | $I_{G_1} + h_1(2h_2A_4 + h_1A_5) + b_1(b_1A_1 - b_2A_2)$ |
| $J_4$ | $I_{G_2} + b_1b_2A_2 + 2h_1h_2A_4 + h_2^2A_6$ | 0 | $I_{G_2} - b_2^2A_2 + h_2^2A_6 - (2b_2h_1A_2 + b_2h_2A_4 + b_1h_2A_4)\sin\lvert\theta_2\rvert + (b_1b_2A_2 + 2h_1h_2A_4 - b_2^2A_2)\cos\lvert\theta_2\rvert$ | $I_{G_2} + b_1b_2A_2 + 2h_1h_2A_4 + h_2^2A_6$ |
| $J_5$ | $(b_1 + b_2)b_2A_2 + 2h_1h_2A_4$ | 0 | $-(b_1h_2A_4 + 2h_1b_2A_2 + b_2h_2A_4)\sin\lvert\theta_2\rvert - (b_2^2A_2 + b_1b_2A_2 - 2h_1h_2A_4)\cos\lvert\theta_2\rvert$ | $I_{G_2} - b_1b_2A_2 + 2h_1h_2A_4 + h_2^2A_6$ |
| $J_6$ | $I_{G_2} - b_2^2A_2 + h_2^2A_6$ | $I_{G_2} - b_2^2A_2 + h_2^2A_6$ | $I_{G_2} + b_2^2A_2 + h_2^2A_6$ | 0 |
| $J_7$ | $(b_1 - b_2)b_2A_2 + 2h_1h_2A_4$ | $(b_1 - b_2)b_2A_2 + 2h_1h_2A_4$ | $(b_1h_2A_4 - 2b_2h_1A_2 - b_2h_2A_4)\sin\lvert\theta_2\rvert - (b_2^2A_2 - b_1b_2A_2 - 2h_1h_2A_4)\cos\lvert\theta_2\rvert$ | $(b_1 - b_2)b_2A_2 + 2h_1h_2A_4$ |
| $J_8$ | $I_{G_2} + b_2^2A_2 + h_2^2A_6$ | $I_{G_2} + b_2^2A_2 + bh_2^2A_6$ | $I_{G_2} + b_2^2A_2 + h_2^2A_6$ | $I_{G_2} + b_2^2A_2 + h_2^2A_6$ |
| | Or from 2a to 3a | Or from 4a to 4b | Or from 2a to 4b | Or from 3a to 3b |
| | Equation (25) | Equation (26) | Equation (26) | Equation (25) |
| $J_1$ | Same as above | 0 | Same as above | Same as above |
| $J_2$ | Same as above | $I_{G_2} - b_2^2A_2 + h_2^2A_6$ | Same as above | Same as above |
| $J_3$ | $I_G + b_1^2A_1 + h^2\,A_8$ | NA | Same as above | $I_G + b_1^2A_1 + h^2\,A_8$ |
| $J_4$ | NA | $I_{G_2} + b_2^2A_2 + h_2^2A_6$ | Same as above | NA |